

1 **A genetically-encoded toolkit of functionalized nanobodies against fluorescent proteins**
2 **for visualizing and manipulating intracellular signalling**

3

4 **David L. Prole^{1,*} and Colin W. Taylor^{1,*}**

5 ¹Department of Pharmacology, University of Cambridge, Tennis Court Road, Cambridge
6 CB2 1PD, United Kingdom

7

8 ***For correspondence:** dp350@cam.ac.uk, cwt1000@cam.ac.uk

9

10 **Short title**

11 Functionalized nanobodies for studying intracellular signalling

12

13 **Keywords:** cell signalling, endoplasmic reticulum, fluorescence microscopy, fluorescent
14 protein, GFP, intrabody, membrane contact site, mitochondria, nanobody, RFP.

15 **Abbreviations**

16 BFP, blue fluorescent protein; $[Ca^{2+}]_c$, cytosolic free Ca^{2+} concentration; CALI,
17 chromophore-assisted light inactivation; CaM, calmodulin; CFP, cyan fluorescent protein;
18 ER, endoplasmic reticulum; FKBP, FK506-binding protein; FRB, FKBP-rapamycin-binding
19 domain; FP, fluorescent protein; GFP, green fluorescent protein; GNb, GFP-binding
20 nanobody; HBS, HEPES-buffered saline; IP₃R, inositol 1,4,5-trisphosphate receptor;
21 LAMP1, lysosomal membrane protein 1; mCherry, monomeric Cherry; MCS, membrane
22 contact site; MHBS, modified HBS; MP, multimerizing protein; mRFP, monomeric red
23 fluorescent protein; OMM, outer mitochondrial membrane; PM, plasma membrane; RFP, red
24 fluorescent protein; RNb, RFP-binding nanobody; ROI, region of interest; SOCE, store-
25 operated Ca^{2+} entry; TIRFM, total internal reflection fluorescence microscopy; YFP, yellow
26 fluorescent protein.

27 **Abstract**

28 **Background:** Intrabodies enable targeting of proteins in live cells, but generating specific
29 intrabodies against the thousands of proteins in a proteome poses a challenge. We leverage
30 the widespread availability of fluorescently labelled proteins to visualize and manipulate
31 intracellular signalling pathways in live cells by using nanobodies targeting fluorescent
32 protein tags.

33 **Results:** We generated a toolkit of plasmids encoding nanobodies against red and green
34 fluorescent proteins (RFP and GFP variants), fused to functional modules. These include
35 fluorescent sensors for visualization of Ca^{2+} , H^+ and ATP/ADP dynamics; oligomerizing or
36 heterodimerizing modules that allow recruitment or sequestration of proteins and
37 identification of membrane contact sites between organelles; SNAP tags that allow labelling
38 with fluorescent dyes and targeted chromophore-assisted light inactivation; and nanobodies
39 targeted to luminal sub-compartments of the secretory pathway. We also developed two
40 methods for crosslinking tagged proteins: a dimeric nanobody, and RFP-targeting and GFP-
41 targeting nanobodies fused to complementary hetero-dimerizing domains. We show various
42 applications of the toolkit and demonstrate, for example, that IP_3 receptors deliver Ca^{2+} to the
43 outer membrane of only a subset of mitochondria, and that only one or two sites on a
44 mitochondrion form membrane contacts with the plasma membrane.

45 **Conclusions:** This toolkit greatly expands the utility of intrabodies, and will enable a range
46 of approaches for studying and manipulating cell signalling in live cells.

47 **Background**

48 Visualizing the location of specific proteins within cells and manipulating their function is
49 crucial for understanding cell biology. Antibodies can define protein locations in fixed and
50 permeabilized cells, but antibodies are large protein complexes that are difficult to introduce
51 into live cells [1]. This limits their ability to interrogate the dynamics or affect the function of
52 proteins in live cells. Small protein-based binders, including nanobodies derived from the
53 variable region of the heavy chains (V_{HH}) of camelid antibodies, offer a promising alternative
54 [2]. Nanobodies can be encoded by plasmids and expressed in live cells. However, generating
55 nanobodies against thousands of protein variants is daunting, and even for single targets it
56 can be time-consuming, costly and not always successful. A solution to this bottleneck is
57 provided by fluorescently tagged proteins, which are widely used in cell biology [3, 4] after
58 heterologous expression of proteins or gene editing of endogenous proteins [5-7]. The most
59 common application of fluorescent protein (FP) tags is to visualize protein locations, but they
60 have additional potential as generic affinity tags to manipulate and visualize protein functions
61 in live cells. These opportunities are under-developed.

62 Green fluorescent protein (GFP) has undergone numerous cycles of optimization as a
63 reporter and non-perturbing tag [3, 8]. Most GFP-tagged proteins therefore retain their
64 endogenous localization and function [9]. Large libraries of plasmids encoding GFP-tagged
65 proteins are now available [10]. Proteome-scale expression of GFP-tagged proteins or
66 genome-scale tagging of gene products with GFP has been reported for *Drosophila* [11],
67 fungi [12-14], plants [15, 16] and bacteria [17].

68 Proteins tagged with red fluorescent proteins (RFPs) such as DsRed, mRFP and mCherry
69 (mCh) are also popular. Extensive optimization has made them attractive tags [3, 18], and
70 libraries of RFP-tagged proteins have been developed in mouse stem cells [19] and yeast
71 [14].

72 Nanobodies that bind to RFP [20, 21] or GFP [21, 22] are most commonly used in their
73 purified forms for immunoprecipitation and immunocytochemistry. However, they also offer
74 a generic means of targeting in live cells the huge variety of available tagged proteins and the
75 many emerging examples of endogenous proteins tagged with FPs by gene editing. GFP-
76 targeting nanobodies have been used for applications such as targeted proteosomal
77 degradation [23, 24] and relocation of proteins in cells [25], but these and other applications
78 are less developed for RFP-targeting nanobodies.

79 Here we develop a plasmid-encoded toolkit of nanobodies that bind common FP tags,
80 including RFPs, CFP, GFP and YFP, fused to functional modules for visualization and
81 manipulation of cell signalling (*Fig. 1*). We fused the nanobodies to a variety of functional
82 modules: fluorescent sensors for Ca^{2+} , H^+ and ATP/ADP; optimized SNAP tags for labelling
83 with bright and photostable dyes [26]; and hetero-dimerizing partners that allow inducible
84 recruitment or sequestration of proteins and visualization of membrane contact sites (MCS)
85 between organelles. We developed two methods to allow crosslinking of RFP-tagged and
86 GFP-tagged proteins: a dimeric nanobody, and co-expression of RFP-targeting and GFP-
87 targeting nanobodies fused to complementary hetero-dimerizing domains. We also describe
88 functionalized nanobodies directed to luminal sub-compartments of the secretory pathway.
89 We demonstrate the utility of nanobody fusions by visualizing local Ca^{2+} dynamics at the
90 surface of mitochondria, by manipulating the locations of proteins and organelles within
91 cells, by characterizing MCS between mitochondria and the plasma membrane (PM), and by
92 targeting luminal Ca^{2+} sensors to a sub-compartment of the endoplasmic reticulum (ER).

93 This versatile toolkit of genetically-encoded, functionalized nanobodies greatly expands
94 the utility of RFP- and GFP-targeting nanobodies. It will provide a valuable resource for
95 studying protein function and cell signalling in live cells. We illustrate some applications and
96 demonstrate, for example, that IP_3 receptors deliver Ca^{2+} to the outer membrane of only some

97 mitochondria and that MCS between mitochondria and the plasma membrane occur at only
98 one or two sites on each mitochondrion.

99

100 **Results**

101 **Targeting RFP and GFP variants with genetically-encoded nanobody fusions in live** 102 **cells**

103 The RFP nanobody (RNb) and GFP nanobody (GNb) used are the previously described llama
104 variants LaM4 and LaG16, respectively [21]. They were chosen for their favourable
105 combinations of high affinity (K_d values of 0.18 nM and 0.69 nM, respectively) and ability to
106 bind a variety of RFP or GFP variants [21]. The latter attribute maximizes their potential for
107 targeting a wide variety of FPs [3, 4]. LaM4 binds both mCh and DsRed variants, but not
108 GFPs [21]. In addition to binding GFP, LaG16 binds cyan, blue and yellow FPs (CFP, BFP
109 and YFP), but not RFPs [21]. In contrast, the widely used VhhGFP4 nanobody binds GFP,
110 but not CFP [22].

111 In HeLa cells with organelles (ER, mitochondria, nucleus and lysosomes) labelled with
112 mCh or mRFP markers, expression of RNb-GFP (*Fig. 2A*) specifically identified the labelled
113 organelle (*Fig. 2B*). Similar results were obtained with GNb-mCh (*Fig. 2C*) and organelles
114 (ER, mitochondria and nucleus) labelled with GFP or mTurquoise (*Fig. 2D*). These results
115 demonstrate that plasmid-encoded RNb and GNb allow specific labelling of a variety of RFP
116 and GFP variants in live cells.

117

118 **Targeting sensors to RFP and GFP**

119 The effects of intracellular messengers such as Ca^{2+} [27], H^+ [28] and ATP/ADP [29] can be
120 highly localized within cells. To enable visualization of these intracellular messengers in

121 microdomains around RFP-tagged and GFP-tagged proteins, we fused RNb and GNb to
122 fluorescent sensors for Ca^{2+} [30], H^+ [31, 32] or ATP/ADP [33].

123 RNb was fused to the green fluorescent Ca^{2+} sensor G-GECO1.2 (**Fig. 3**), and GNb was
124 fused to the red fluorescent Ca^{2+} sensors, R-GECO1.2 or LAR-GECO1.2 [30] (**Fig. 4**). The
125 affinities of these sensors for Ca^{2+} (K_D^{Ca} of 1.2 μM for G-GECO1.2 and R-GECO1.2, and 10
126 μM for LAR-GECO1.2) are low relative to global changes in the cytosolic free Ca^{2+}
127 concentration ($[\text{Ca}^{2+}]_c$) after receptor stimulation (typically ~ 300 nM) [34]. This facilitates
128 selective detection of the large, local rises in $[\text{Ca}^{2+}]$ that are important for intracellular
129 signalling, at the contacts between active inositol 1,4,5-trisphosphate receptors (IP_3Rs) and
130 mitochondria, for example [27]. To allow targeted measurement of relatively low resting
131 $[\text{Ca}^{2+}]$ within cellular microdomains we also fused RNb to the ratiometric Ca^{2+} -sensor, GEM-
132 GECO1 ($K_D^{\text{Ca}} = 300$ nM) [30], to give RNb-GEMGECO1 (**Additional file 1: Fig. S1**).

133 In HeLa cells expressing TOM20-mCh or TOM20-GFP to identify the outer mitochondrial
134 membrane (OMM), the RNb- Ca^{2+} sensors (**Fig. 3** and **Additional file 1: Fig. S1**) and GNb-
135 Ca^{2+} sensors (**Fig. 4**) were targeted to the OMM. Both families of targeted sensor reported an
136 increase in $[\text{Ca}^{2+}]$ after treatment with the Ca^{2+} ionophore, ionomycin (**Fig. 3**, **Fig. 4** and
137 **Additional file 1: Fig. S1**). This confirms the ability of the sensors to report $[\text{Ca}^{2+}]$ changes
138 when targeted to the OMM microdomain.

139 In some cells, the targeted Nb- Ca^{2+} sensors revealed local changes in $[\text{Ca}^{2+}]_c$ after receptor
140 stimulation with histamine, which stimulates IP_3 formation and Ca^{2+} release from the ER in
141 HeLa cells [34]. Imperfect targeting of the RNb-GGECO1.2 to the OMM allowed Ca^{2+}
142 signals at the surface of individual mitochondria to be distinguished from those in nearby
143 cytosol in some cells (**Fig. 3D-F** and **Additional file 2: Video 1**). In the example shown,
144 RNb-GGECO1.2 at both the OMM and nearby cytosol responded to the large, global
145 increases in $[\text{Ca}^{2+}]$ evoked by ionomycin. However, cytosolic RNb-GGECO1.2 did not

146 respond to histamine, while the sensor at the OMM responded with repetitive spiking (**Fig.**
147 **3D-F** and **Additional file 2: Video 1**). The GNb-LARGE1.2 sensor, which has the lowest
148 affinity for Ca^{2+} of the sensors used, revealed changes in $[\text{Ca}^{2+}]_c$ at the surface of some
149 mitochondria, but not others in the same cell (**Fig. 4D-F**, **Fig. 4H** and **Additional file 3:**
150 **Video 2**). In the example shown, GNb-LARGE1.2 at the OMM in all mitochondria within
151 the cell responded to the large, global increases in $[\text{Ca}^{2+}]$ evoked by ionomycin. However, in
152 response to histamine mitochondria in the perinuclear region responded, but not those in
153 peripheral regions (**Fig. 4D-F**, **Fig. 4H** and **Additional file 3: Video 2**). Ca^{2+} uptake by
154 mitochondria affects many cellular responses, including mitochondrial metabolism, ATP
155 production and apoptosis [35]; and Ca^{2+} at the cytosolic face of the OMM regulates
156 mitochondrial motility [36]. The subcellular heterogeneity of mitochondrial exposure to
157 increased $[\text{Ca}^{2+}]$ suggests that these responses may be very localized in cells.

158 These observations align with previous reports showing that Ca^{2+} -mobilizing receptors
159 evoke both oscillatory $[\text{Ca}^{2+}]$ changes within the mitochondrial matrix [37], and large local
160 increases in $[\text{Ca}^{2+}]$ at the cytosolic face of the OMM [38]. Our results establish that
161 nanobody- Ca^{2+} -sensor fusions are functional and appropriately targeted, and can be used to
162 detect physiological changes in $[\text{Ca}^{2+}]$ within cellular microdomains such as the OMM.

163 For targeted measurements of intracellular pH, RNb was fused to the green fluorescent pH
164 sensor super-ecliptic pHluorin (SEpHluorin) [31], and GNb was fused to the red fluorescent
165 pH sensor pHuji [32]. Both Nb-pH sensors were targeted to the OMM by the appropriate
166 fluorescent tags, where they responded to changes in intracellular pH imposed by altering
167 extracellular pH in the presence of the H^+/K^+ ionophore nigericin (**Fig. 5**).

168 For targeted measurements of ATP/ADP, RNb was fused to the excitation-ratiometric
169 ATP/ADP sensor Perceval-HR [33]. RNb-Perceval-HR was targeted to the surface of

170 mitochondria and responded to inhibition of glycolysis and oxidative phosphorylation (*Fig.*
171 *6*).

172 The results demonstrate that nanobodies can be used to direct sensors for Ca^{2+} , H^+ or
173 ATP/ADP to specific subcellular compartments tagged with variants of RFP or GFP.

174

175 **Targeting SNAPf tags to RFP and GFP in live cells**

176 SNAP, and related tags, are versatile because a range of SNAP substrates, including some
177 that are membrane-permeant, can be used to attach different fluorophores or cargoes to the
178 tag [39]. Purified GFP-targeting nanobodies fused to a SNAP tag have been used to label
179 fixed cells for optically demanding applications [40]. We extended this strategy to live cells
180 using RNb and GNb fused to the optimized SNAPf tag [41] (*Fig. 7A* and *B*). In cells
181 expressing the mitochondrial marker TOM20-mCh, RNb-SNAPf enabled labelling of
182 mitochondria with the cell-permeable substrate SNAP-Cell 647-SiR and imaging at far-red
183 wavelengths (*Fig. 7C*). In cells expressing lysosomal LAMP1-mCh and RNb-SNAPf, SNAP-
184 Cell 647-SiR instead labelled lysosomes (*Fig. 7D*), demonstrating that SNAP-Cell 647-SiR
185 specifically labelled the organelles targeted by RNb-SNAPf. Similar targeting of SNAP-Cell
186 647-SiR to mitochondria (*Fig. 7E*) and lysosomes (*Fig. 7F*) was achieved by GNb-SNAPf
187 co-expressed with the appropriate GFP-tagged organelle markers.

188 Chromophore-assisted light inactivation (CALI) can inactivate proteins or organelles by
189 exciting fluorophores attached to them that locally generate damaging reactive superoxide.
190 Historically, antibodies were used to direct a photosensitizer to its target, but fusion of
191 fluorescent proteins or SNAP tags to proteins of interest is now widely used [42]. RNb-
192 SNAPf and GNb-SNAPf make the SNAP strategy more broadly applicable to CALI
193 applications. We demonstrate this by targeting CALI to the outer surface of lysosomes. We
194 anticipated that CALI in this microdomain might, amongst other effects, disrupt the motility

195 of lysosomes, which depends on their association with molecular motors [43]. RNb-SNAPf
196 enabled labelling of lysosomes with the CALI probe fluorescein, using the cell-permeable
197 substrate, SNAP-Cell-fluorescein (**Fig. 8A and B**). Exposure to blue light then immobilized
198 the lysosomes (**Fig. 8C-F** and **Additional file 4: Video 3**), indicating a loss of motor-driven
199 motility. Control experiments demonstrated that labelling cytosolic SNAPf with SNAP-Cell-
200 fluorescein (**Additional file 1: Fig. S2A and S2B**) had significantly less effect on lysosomal
201 motility after exposure to blue light (**Fig. 8F** and **Additional file 1: Fig. S2C-E**). These
202 results demonstrate that nanobody-SNAPf fusions allow targeting of fluorescent dyes in live
203 cells, which can be used for re-colouring of tagged proteins or targeted CALI.

204

205 **Sequestration of proteins tagged with RFP or GFP**

206 Fusion of GFP nanobodies to degrons allows proteasomal degradation of GFP-tagged
207 proteins [24], but the method is slow and cumbersome to reverse. An alternative strategy is to
208 sequester tagged proteins so they cannot fulfil their normal functions. We used two strategies
209 to achieve this: artificial clustering and recruitment to mitochondria.

210 We induced artificial clustering by fusing RNb or GNb to a multimerizing protein (MP)
211 comprising a dodecameric fragment of Ca²⁺-calmodulin-dependent protein kinase II
212 (CaMKII) [44], with an intervening fluorescent protein (mRFP or mCerulean) for
213 visualization of the Nb fusion (**Fig. 9A and B**). RNb-mCerulean-MP caused clustering of the
214 ER transmembrane protein mCh-Sec61β (**Fig. 9C and D**) and caused lysosomes tagged with
215 LAMP1-mCh to aggregate into abnormally large structures (**Fig. 9E and F**). GNb-mRFP-MP
216 had the same clustering effect on lysosomes labelled with LAMP1-GFP (**Fig. 9G and H**) and
217 caused clustering of GFP-tagged proteins in the cytosol (calmodulin, **Fig. 9I and J**), nucleus
218 and cytosol (p53, **Fig. 9K and L**) or ER membranes (IP₃R3, **Fig. 9M and N**).

219 For inducible sequestration, sometimes known as ‘knocksideways’ [45], we used two
220 approaches based on hetero-dimerizing modules, one chemical and one optical. First, we
221 adapted the original knocksideways method, where proteins tagged with FKBP (FK506-
222 binding protein) are recruited by rapamycin to proteins tagged with FRB (FKBP-rapamycin-
223 binding domain) on the OMM, and thereby sequestered. The method has hitherto relied on
224 individual proteins of interest being tagged with FKBP [45]. RNb-FKBP and GNb-FKBP
225 (**Fig. 10A** and **B**) extend the method to any protein tagged with RFP or GFP. For our
226 analyses, we expressed TOM70 (an OMM protein) linked to FRB through an intermediary
227 fluorescent protein (GFP or mCh, to allow optical identification of the fusion protein). RNb-
228 FKBP sequestered the ER transmembrane protein mCh-Sec61 β at the OMM (TOM70-GFP-
229 FRB) within seconds of adding rapamycin (**Additional file 5: Video 4**) and rapidly depleted
230 mCh-Sec61 β from the rest of the ER (**Fig. 10C-E**). After addition of rapamycin, GNb-FKBP
231 rapidly sequestered endogenous IP₃R1 tagged with GFP (GFP-IP₃R1) [7] (**Fig. 10F** and **G**,
232 and **Additional file 6: Video 5**) and cytosolic GFP-tagged calmodulin (**Fig. 10H** and
233 **Additional file 7: Video 6**) at mitochondria expressing TOM70-mCh-FRB. Rapamycin
234 caused no sequestration in the absence of the nanobody fusions (**Additional file 1: Fig. S3**).

235 To make sequestration reversible and optically activated, we adapted the light-oxygen-
236 voltage-sensing domain (LOV2)/Zdark (zdk1) system in which light induces dissociation of
237 LOV2-zdk1 hetero-dimers [46]. Because this system is operated by blue light at intensities
238 lower than required for imaging GFP [46], it is most suitable for use with red fluorescent
239 tags. RNb-zdk1 (**Fig. 11A**) sequestered cytosolic mCh on the OMM in cells expressing
240 TOM20-LOV2, and blue laser light rapidly and reversibly redistributed mCh to the cytosol
241 (**Fig. 11B** and **C**).

242

243

244 **Inducible recruitment of tagged proteins to membrane contact sites**

245 The ability of Nb-FKBP fusions to recruit membrane proteins to FRB-tagged targets
246 suggested an additional application: revealing contact sites between membrane-bound
247 organelles. ER-mitochondrial membrane contact sites (MCS) have been much studied [47],
248 but contacts between the PM and mitochondria, which are less extensive [48], have received
249 less attention. In HeLa cells co-expressing the PM β_2 -adrenoceptor tagged with mCh (β_2 AR-
250 mCh), TOM20-GFP-FRB and RNb-FKBP, rapamycin caused rapid recruitment of β_2 AR-
251 mCh within the PM to mitochondria at discrete puncta that grew larger with time (**Fig. 12A-E**
252 and **Additional file 8: Video 7**). Recruitment was not seen in the absence of co-expressed
253 RNb-FKBP (**Fig. 12F**). Rapamycin also triggered similar punctate accumulation of β_2 AR at
254 mitochondria in COS-7 cells expressing β_2 AR-GFP, TOM20-mCh-FRB and GNb-FKBP
255 (**Additional file 1: Fig. S4**). In similar analyses of ER-mitochondria and PM-mitochondria
256 MCS, the initial punctate colocalization of proteins was shown to report native MCS, which
257 grew larger with time as rapamycin zipped the proteins together [48]. Our results are
258 consistent with that interpretation. In most cases, β_2 AR were recruited to only one or two
259 discrete sites on each mitochondrion, which expanded during prolonged incubation with
260 rapamycin, but without the appearance of new sites (**Fig. 12D and E**, and **Additional file 1:**
261 **Fig. S4**). Rapamycin had no evident effect on recruiting new mitochondria to the PM, but it
262 did cause accumulation of tagged TOM70 at MCS and depletion of TOM70 from the rest of
263 each mitochondrion, indicating mobility of TOM70 within the OMM (**Additional file 1: Fig.**
264 **S4**). Our results suggest that inducible cross-linking using RNb-FKBP or GNb-FKBP
265 identifies native MCS between mitochondria and PM, with each mitochondrion forming only
266 one or two MCS with the PM. We have not explored the functional consequences of these
267 restricted MCS, but we speculate that they may identify sites where proteins involved in
268 communication between the PM and mitochondria are concentrated, facilitating, for example,

269 phospholipid transfer [49], the generation of ATP microdomains [50], or Ca^{2+} exchanges
270 between mitochondria and store-operated Ca^{2+} entry (SOCE) [51] or PM Ca^{2+} -ATPases [52].

271 We next tested whether PM proteins could be recruited to the MCS between ER-PM that
272 are important for SOCE and lipid transfer [53]. In response to rapamycin, mCh-Orai1, the
273 PM Ca^{2+} channel that mediates SOCE [54], was recruited by RNb-FKBP to ER-PM MCS
274 labelled with the marker GFP-MAPPER-FRB [55] (*Fig. 13A and B*). Recruitment was not
275 observed in the absence of RNb-FKBP (*Fig. 13C*). We conclude that the method identifies
276 native ER-PM MCS during the initial phase of Nb recruitment, and the Nb subsequently
277 exaggerates these MCS.

278 One of the least explored MCS is that between lysosomes and mitochondria [56]. Recent
279 evidence shows that these MCS control the morphology of both organelles [57] and probably
280 mediate exchange of cholesterol and other metabolites between them [58]. We assessed
281 whether the nanobody fusions could be used to inducibly recruit lysosomes to mitochondria.
282 GNb-FKBP enabled recruitment of lysosomes labelled with LAMP1-GFP to mitochondria
283 labelled with TOM20-mCh-FRB, in response to rapamycin (*Fig. 14A-C*). Lysosomes were
284 not recruited to mitochondria in the absence of GNb-FKBP (*Fig. 14D*).

285

286 **Cross-linking RFP-tagged and GFP-tagged proteins**

287 We generated a dimeric nanobody (GNb-RNb) that binds simultaneously to GFP and RFP
288 (*Fig. 15A*), and demonstrated its utility by crosslinking a variety of GFP-tagged and RFP-
289 tagged proteins. Cytosolic GFP, normally diffusely distributed in the cytosol (data not
290 shown), was recruited to nuclei by H2B-mCh (*Fig. 15B*) or to mitochondria by TOM20-mCh
291 (*Fig. 15C*). In the presence of GNb-RNb, mCh-Orai1 and endogenously tagged GFP-IP₃R1
292 formed large co-clusters (*Fig 15D*) that differed markedly from the distributions of GFP-
293 IP₃R1 (*Fig. 10F*) and mCh-Orai1 (*Fig 13*) in the absence of crosslinking. Consistent with

294 earlier results (*Fig. 12* and *Additional file 1: Fig. S4*), β_2 AR-mCh, which is normally
295 diffusely distributed in the PM, formed mitochondria-associated puncta when crosslinked to
296 mitochondria expressing TOM20-GFP (*Fig. 15E*). Whole organelles could also be
297 crosslinked. Co-expression of LAMP1-GFP and LAMP1-mCh labelled small, mobile
298 lysosomes in control cells (*Fig. 15F*), while additional co-expression of GNb-RNb caused
299 accumulation of lysosomes into large clusters (*Fig. 15G*).

300 This crosslinking of GFP and RFP was made rapidly inducible with an RNb-FRB fusion
301 that hetero-dimerizes with GNb-FKBP in the presence of rapamycin (*Fig. 16A*). Co-
302 expression of GNb-FKBP with RNb-FRB in cells co-expressing TOM20-GFP and mCh-
303 Sec61 β led to rapid colocalization of GFP and mCh after addition of rapamycin (*Fig. 16B*
304 and *C*, and *Additional file 9: Video 8*). Similar results were obtained with RNb-FKBP and
305 GNb-FRB (*Additional file 1: Fig. S5*). We conclude that GNb-FKBP and RNb-FRB provide
306 a rapidly inducible system for crosslinking any GFP-tagged protein to any RFP-tagged
307 protein.

308

309 **Targeting secretory compartments with luminal nanobodies**

310 GNb and RNb were directed to the lumen of the secretory pathway by addition of an N-
311 terminal signal sequence, giving ssGNb and ssRNb. Targeting of ssGNb-mCh to the Golgi,
312 ER network, or ER-PM MCS was achieved by co-expression of organelle markers with
313 luminal FP tags (*Fig. 17A* and *B*). In each case, there was significant colocalization of green
314 and red proteins. Similar targeting of ssRNb-GFP to the ER network or ER-PM MCS was
315 achieved by co-expression with mCh-tagged luminal markers of these organelles (*Fig. 17C*
316 and *D*). These results demonstrate that ssGNb and ssRNb fusions can be directed to the
317 lumen of specific compartments of the secretory pathway.

318 Fluorescent Ca²⁺ sensors targeted to the lumen of the entire ER [59, 60] are widely used
319 and have considerably advanced our understanding of Ca²⁺ signalling [61, 62]. Fluorescent
320 Ca²⁺ sensors targeted to ER sub-compartments and the secretory pathway have received less
321 attention but have, for example, been described for the Golgi [63, 64]. Our nanobody
322 methods suggest a generic approach for selective targeting of luminal Ca²⁺ indicators. Fusion
323 of ssRNb to GCEPIA1 or GEM-CEPIA [60] provided ssRNb-GCEPIA1 and ssRNb-
324 GEMCEPIA (*Fig. 18A*). These fusions were targeted to the luminal aspect of ER-PM
325 junctions by co-expression with mCh-MAPPER [7] (*Fig. 18C and D*). Fusion of ssGNb to
326 the low-affinity Ca²⁺ sensors LAR-GECO1 [59] or RCEPIA1 [60] provided ssGNb-
327 LARGECO1 and ssGNb-RCEPIA1 (*Fig. 18B*). These fusions allowed targeting to ER-PM
328 junctions labelled with GFP-MAPPER (*Fig. 18E and F*). The targeted Ca²⁺ sensors
329 responded appropriately to emptying of intracellular Ca²⁺ stores by addition of ionomycin in
330 Ca²⁺-free medium (*Fig. 18G-K*). These results confirm that Ca²⁺ sensors targeted to a
331 physiologically important ER sub-compartment, the ER-PM junctions where SOCE occurs,
332 report changes in luminal [Ca²⁺]. Our results demonstrate that nanobody fusions can be
333 targeted to luminal sub-compartments of the secretory pathway and they can report [Ca²⁺]
334 within physiologically important components of the ER.

335

336 **Discussion**

337 The spatial organization of the cell interior influences all cellular activities and it is a
338 recurrent theme in intracellular signalling [65, 66]. Hence, tools that can visualize and
339 manipulate the spatial organization of intracellular components are likely to find widespread
340 application. We introduce a toolkit of plasmids encoding functionalized nanobodies against
341 common FP tags, including CFP, GFP, YFP and RFPs (*Fig. 1*). Use of this toolkit is
342 supported by genome-wide collections of plasmids, cells and organisms expressing proteins

343 tagged with GFP and RFP [10-17, 19], and by facile methods for heterologous expression of
344 tagged proteins or editing of endogenous genes to encode FP tags [5, 6]. The functionalized
345 nanobodies provide new approaches to studying intracellular signalling in live cells.

346 Our toolkit expands the repertoire of functionalized RFP-binding nanobodies, which are
347 less developed than their GFP-binding counterparts [67]. The RNb fusions provide new
348 opportunities to use RFP, which often has advantages over GFP. For example, RFP is
349 spectrally independent from blue-green sensors, which are usually superior to their red
350 counterparts [30, 32]; from the CALI probe, fluorescein; and from optogenetic modules,
351 which are often operated by blue-green light [68].

352 Nanobody-sensor fusions allow targeting of sensors to specific proteins and organelles
353 (**Figs. 2-6**), and will aid visualization of signalling within cellular microdomains. Fusion of
354 nanobodies to the Ca^{2+} sensors G-GECO1.2, R-GECO1.2 and LAR-GECO1.2 [30] (**Figs. 3**
355 **and 4**), which have relatively low affinities for Ca^{2+} (K_D values of 1.2 μM , 1.2 μM and 10
356 μM , respectively), should facilitate selective detection of the relatively large, local rises in
357 $[\text{Ca}^{2+}]_c$ that are important for cell signalling [27]. The GEM-GECO Ca^{2+} sensor [30], H^+
358 sensors [31, 32] and ATP/ADP sensors [33] used for nanobody fusions are poised to detect
359 fluctuations of their ligands around resting concentrations in the cell (**Figs. 4-6**).

360 Relative to direct fusions of sensors to proteins of interest, nanobody-sensor fusions have
361 several advantages. Firstly, the generic nanobody toolkit (**Fig. 1**) can be combined with
362 collections of FP-tagged proteins to provide many combinations; each would otherwise
363 require expression of a unique construct that may or may not function normally. Secondly,
364 each sensor is attached to the same entity (nanobody), which binds to the same partner (FP).
365 Since the biophysical and biochemical properties of sensors may be influenced by their
366 fusion partners, this provides greater confidence that sensors dispatched to different locations
367 will respond similarly to their analyte.

368 Nanobodies allow re-colouring of FPs with alternative fluorophores that may have
369 advantageous properties. For example, recolouring of RFP-tagged proteins with RNb-GFP
370 (**Fig. 2B**) enables visualization of organelles with GFP, which has enhanced photophysical
371 properties relative to RFPs. Nanobody-SNAPf fusions can be used to attach fluorescent dyes,
372 including CALI probes and far-red fluorophores, to FP tags (**Figs. 7 and 8**). Longer excitation
373 wavelengths cause less phototoxicity and allow greater penetration through tissue, which may
374 be useful in studies of transgenic organisms and tissues. We also envisage live-cell
375 applications in pulse-chase analyses and using super-resolution microscopy, Förster
376 resonance energy transfer (FRET) and fluorescence lifetime imaging.

377 Membrane-permeant forms of the SNAP ligand, O⁶-benzylguanine, are available
378 conjugated to conventional Ca²⁺ indicators (Fura-2FF, Indo-1 and BOCA-1), which are
379 brighter than genetically-encoded indicators [69-71]; to derivatives of the two-photon
380 fluorophore naphthalimide [72]; to the hydrogen peroxide sensor
381 nitrobenzoylcarbonylfluorescein [73]; and to reversible chemical dimerizers [74, 75].
382 Nanobody-SNAPf fusions will allow facile targeting of these modules to any protein or
383 organelle tagged with RFP or GFP.

384 Cross-linking methods have many applications in cell biology, including stabilizing
385 protein interactions (eg, for pull-downs), identifying and manipulating MCS, enforcing
386 protein interactions (eg, receptor dimerization), redirecting proteins to different subcellular
387 locations (eg, knocksideways) and many more. Functionalized nanobodies provide many
388 additional opportunities to regulate protein associations. The nanobody-FKBP/FRB fusions,
389 for example, allow rapid rapamycin-mediated crosslinking of any pair of proteins tagged with
390 GFP/RFP, or tagged with either FP and any of the many proteins already tagged with FKBP
391 or FRB [76] (**Figs. 10 and 12-16**). Nanobody-FKBP fusions may allow crosslinking to
392 SNAP-tagged proteins [75], and the nanobody-SNAPf fusions to HaloTag-tagged proteins

393 [74] and FKBP-tagged proteins [75]. RNb-zdk1 fusions allow photo-inducible crosslinking of
394 RFP-tagged proteins to LOV-tagged proteins [46] (**Fig. 11**). Nanobodies that crosslink GFP-
395 tagged proteins to RFP-tagged proteins (GNb-RNb; and the GNb-FKBP/RNb-FRB and GNb-
396 FRB/RNb-FKBP pairings) may have the most applications, as they can take fullest advantage
397 of the numerous combinations of existing RFP and GFP-tagged proteins (**Figs. 15 and 16**).

398 Functionalized nanobodies directed to luminal compartments of the secretory pathway
399 would provide useful tools, but they are under-developed. Their potential is shown by
400 nanobodies retained within the ER, which restrict onward trafficking of target proteins and
401 inhibit their function [77]. We show that functionalized nanobodies, including nanobody-Ca²⁺
402 sensors, can be directed to sub-compartments of the secretory pathway (**Figs. 17 and 18**).
403 Luminal Ca²⁺ provides a reservoir within the ER, Golgi and lysosomes that can be released
404 by physiological stimuli to generate cytosolic Ca²⁺ signals [78, 79]. Compartmentalization of
405 Ca²⁺ stores within the ER [63] and Golgi [79] adds to the complexity of luminal Ca²⁺
406 distribution in cells. Furthermore, luminal Ca²⁺ itself regulates diverse aspects of cell
407 biology, including SOCE [54], sorting of cargo in the Golgi [80], binding of ERGIC-53 to
408 cargoes within the ER-Golgi intermediate compartment (ERGIC) [81], and exocytosis of
409 neurotransmitters by secretory vesicles [82, 83]. Hence, there is a need for tools that can
410 effectively report luminal [Ca²⁺] within this complex luminal environment. The luminal
411 nanobody-Ca²⁺ sensors detected changes in luminal [Ca²⁺] at the ER-PM MCS where SOCE
412 occurs (**Fig. 18**).

413 In addition to nanobodies, other protein-based binders, including single-domain
414 antibodies, designed ankyrin-repeat proteins (DARPINs), affimers, anticalins, affibodies and
415 monobodies have been developed to recognise many important intracellular proteins [2, 84-
416 86]. These binding proteins can be easily transplanted into the fusion scaffolds described to
417 maximize their exploitation.

418

419 **Conclusions**

420 We present a toolkit of plasmids encoding functionalized nanobodies directed against
421 common fluorescent protein tags, which will allow a wide range of applications and new
422 approaches to studying intracellular signalling in live cells. We illustrate some applications
423 and demonstrate, for example, that IP₃ receptors deliver Ca²⁺ to the OMM of only some
424 mitochondria, and that MCS between mitochondria and the plasma membrane occur at only
425 one or two sites on each mitochondrion.

426

427 **Materials and Methods**

428

429 **Materials**

430 Human fibronectin was from Merck Millipore. Ionomycin was from Apollo Scientific
431 (Stockport, UK). Rapamycin was from Cambridge Bioscience (Cambridge, UK). SNAP
432 substrates were from New England Biolabs (Hitchin, UK). Other reagents, including
433 histamine and nigericin, were from Sigma-Aldrich.

434

435 **Plasmids**

436 Sources of plasmids encoding the following proteins were: mCherry-C1 (Clontech
437 #632524); mCherry-N1 (Clontech #632523); EGFP-N1 (Clontech #6085-1); GFP-ERcyt,
438 mCherry-ERcyt and mTurquoise2-ERcyt (GFP, mCherry or mTurquoise2 targeted to the
439 cytosolic side of the ER membrane via the ER-targeting sequence of the yeast UBC6
440 protein) [87]; mCherry-ERlumen (Addgene #55041, provided by Michael Davidson);
441 LAMP1-mCherry [88]; TPC2-mRFP [89]; TOM20-mCherry (Addgene #55146, provided
442 by Michael Davidson); CIB1-mRFP-MP (Addgene #58367) [44]; CIB1-mCerulean-MP

443 (Addgene #58366) [44]; H2B-GFP (Addgene #11680) [90]; TOM20-LOV2 (Addgene
444 #81009) [46]; mCherry-Sec61 β [91]; GFP-MAPPER [55]; GFP-CaM (Addgene #47602,
445 provided by Emanuel Strehler); TOM70-mCherry-FRB (pMito-mCherry-FRB, Addgene
446 #59352) [92]; pmTurquoise2-Golgi (Addgene #36205) [93]; pTriEx-mCherry-zdk1
447 (Addgene #81057) [46]; pTriEx-NTOM20-LOV2 (Addgene #81009) [46]; β_2 AR-mCFP
448 (Addgene #38260) [94]; pCMV-G-CEPIA1er (Addgene #58215) [60]; pCMV-R-CEPIA1er
449 (Addgene #58216) [60]; pCIS-GEM-CEPIA1er (Addgene #58217) [60]; CMV-ER-LAR-
450 GECO1 and CMV-mito-LAR-GECO1.2 [59]; mCherry-MAPPER and mCherry-Orai1 [7].

451 H2B-mCh was made by transferring H2B from H2B-GFP to pmCherry-N1 (Clontech)
452 using *KpnI/BamHI*. LAMP1-GFP was made by transferring LAMP1 from LAMP1-
453 mCherry into pEGFP-N1 (Clontech) using *EcoRI/BamHI*. β_2 AR-mCherry was made by
454 transferring β_2 AR from β_2 AR-mCFP to pmCherry-N1 (Clontech) using *NheI/XhoI*. β_2 AR-
455 GFP was made by transferring GFP from pEGFP-N1 (Clontech) into β_2 AR-mCherry using
456 *XhoI/NotI*. The mCherry-Golgi plasmid was made by transferring mCherry from
457 pmCherry-N1 into pEYFP-Golgi (Clontech) using *AgeI/NotI*. GFP-Golgi was made by
458 transferring GFP from pEGFP-N1 (Clontech) into Golgi-mCherry using *AgeI/NotI*.
459 TOM20-GFP was made by transferring EGFP from pEGFP-N1 into TOM20-mCherry
460 using *BamHI/NotI*. TOM70-GFP-FRB was made by insertion of EGFP from pEGFP-N1 into
461 TOM70-mCh-FRB using *AgeI/BsrGI*. SNAPf-pcDNA3.1(+) was made by transferring
462 SNAPf from pSNAPf (New England Biolabs) to pcDNA3.1 (+) using *NheI/NotI*.

463 DNA constructs encoding GNb and RNb were synthesized as DNA Strings
464 (ThermoFisher) and introduced by Gibson assembly (Gibson Assembly Master Mix, New
465 England Biolabs) into pcDNA3.1(+) digested with *BamHI/EcoRI*. Sequences encoding
466 GNb and RNb are shown in **Additional file 1: Fig. S6**. Plasmids encoding nanobody
467 fusion constructs (**Fig. 1**) were constructed from the GNb and RNb plasmids using PCR,

468 restriction digestion and ligation, or synthetic DNA Strings and Gibson assembly, and
469 their sequences were confirmed.

470 GNB-mCherry was made by PCR of pmCherry-N1 using forward
471 (ACTGGATCCATGGTGAGCAAGGGCGAG) and reverse
472 (GTACTCGAGCTACTTGTACAGCTCGTCCATGC) primers, followed by insertion into
473 GNB-pcDNA3.1(+) using *Bam*HI/*Xho*I. RNB-GFP was made by PCR of pEGFP-N1 using
474 forward (ACTGGATCCATGGTGAGCAAGGGCGAG) and reverse
475 (GTACTCGAGCTACTTGTACAGCTCGTCCATGC) primers, followed by insertion into
476 RNB-pcDNA3.1(+) using *Bam*HI/*Xho*I. RNB-mCerulean-MP was made by PCR of RNB
477 using forward (ATGCTAGCAAGCTTGCCACCATGGCTC) and reverse
478 (ATACCGGTGAGGATCCAGAGCCTCCGC) primers, followed by insertion into CIB1-
479 mCerulean-MP using *Nhe*I/*Age*I. GNB-mRFP-MP was made by PCR of GNB-FKBP with
480 forward (TAGCTAGCGCCACCATGGCTCAGGTG) and reverse
481 (CGACCGGTACGGACACGGTCACTTGGG) primers, and insertion into CIB1-mRFP1-
482 MP using *Nhe*I/*Age*I. GNB-SNAPf and RNB-SNAPf were made by PCR of GNB-
483 pcDNA3.1(+) and RNB-pcDNA3.1(+) using forward
484 (CAGCTAGCTTGGTACCGAGCTCAAGCTTGC) and reverse
485 (ATGAATTCAGATCCCCCTCCGCCAC) primers, followed by insertion into SNAPf-
486 pcDNA3.1 (+) using *Nhe*I/*Eco*RI. GNB-LAR-GECO1.2 was made by PCR of CMV-mito-
487 LAR-GECO1.2 using forward (CAGGATCCATGGTCGACTCTTCACGTCGTAAGTGG)
488 and reverse (GTACTCGAGCTACTTCGCTGTCATCATTTGTACAAACT) primers,
489 followed by insertion into GNB-pcDNA3.1(+) using *Bam*HI/*Xho*I. RNB-GGECO1.2 was
490 made by PCR of CMV-G-GECO1.2 using forward
491 (CAGGATCCATGGTCGACTCATCACGTCGTAAG) and reverse
492 (TACGATGGGCCCTACTTCGCTGTCATCATTTGTACAAACTCTTC) primers,

493 followed by insertion into RNb-pcDNA3.1(+) using *Bam*HI/*Apa*I. RNb-Perceval-HR was
494 made by PCR of Perceval-HR with forward
495 (AAGCGGCCGCTATGAAAAAGGTTGAATCCATCATCAGGCC) and reverse
496 (ATCTCGAGTCACAGTGCTTCCTTGCCCTC) primers, followed by insertion into RNb-
497 pcDNA3.1(+) using *Not*I/*Xho*I.

498 ss-GNb-mCherry was made by inserting mCherry from GNb-mCherry into ss-GNb-
499 FKBP using *Bam*HI/*Not*I. ss-RNb-GFP was made by inserting GFP from RNb-GFP into ss-
500 RNb-pcDNA3.1(+) using *Bam*HI/*Not*I. ss-GNb-RCEPIA was made by transferring RCEPIA
501 from pCMV-R-CEPIA1er to ss-RNb-pcDNA3.1(+) using *Bam*HI/*Not*I. ss-GNb-LAR-
502 GECO1 was made by transferring a DNA String encoding ss-GNb into CMV-ER-LAR-
503 GECO1 using *Hind*III/*Bam*HI. ss-RNb-GCEPIA was made by transferring GCEPIA from
504 pCMV-G-CEPIA1er to ss-RNb-pcDNA3.1(+) using *Bam*HI/*Not*I. ss-RNb-GEMCEPIA was
505 made by transferring GEM-CEPIA from pCIS-GEM-CEPIA1er to ss-RNb-pcDNA3.1(+)
506 using *Bam*HI/*Not*I.

507

508 **Cell culture and transient transfection**

509 HeLa and COS-7 cells (American Type Culture Collection) were cultured in Dulbecco's
510 modified Eagle's medium/F-12 with GlutaMAX (ThermoFisher) supplemented with foetal
511 bovine serum (FBS, 10%, Sigma). Cells were maintained at 37°C in humidified air with
512 5% CO₂, and passaged every 3-4 days using Gibco TrypLE Express (ThermoFisher). For
513 imaging, cells were grown on 35-mm glass-bottomed dishes (#P35G-1.0-14-C, MatTek)
514 coated with human fibronectin (10 µg.ml⁻¹). Cells were transfected, according to the
515 manufacturer's instructions, using TransIT-LT1 (GeneFlow) (1 µg DNA per 2.5 µl
516 reagent). Short tandem repeat profiling (Eurofins, Germany) was used to authenticate the

517 identity of HeLa cells [7]. Screening confirmed that all cells were free of mycoplasma
518 infection.

519

520 **Fluorescence microscopy and analysis**

521 Cells were washed prior to imaging at 20°C in HEPES-buffered saline (HBS: NaCl 135
522 mM, KCl 5.9 mM, MgCl₂ 1.2 mM, CaCl₂ 1.5 mM, HEPES 11.6 mM, D-glucose 11.5 mM,
523 pH 7.3). Ca²⁺-free HBS lacked CaCl₂ and contained EGTA (1 mM). For manipulations of
524 intracellular pH, cells were imaged in modified HBS (MHBS: KCl 140 mM, MgCl₂ 1.2
525 mM, CaCl₂ 1.5 mM, HEPES 11.6 mM, D-glucose 11.5 mM, pH 7.2). The H⁺/K⁺ ionophore
526 nigericin (10 µM) was added 5 min before imaging to equilibrate intracellular and
527 extracellular pH, and the extracellular pH was then varied during imaging by exchanging
528 the MHBS (pH 6.5 or pH 8).

529 Fluorescence microscopy was performed at 20°C as described previously [7] using an
530 inverted Olympus IX83 microscope equipped with a 100× oil-immersion TIRF objective
531 (numerical aperture, NA 1.49), a multi-line laser bank (425, 488, 561 and 647 nm) and an
532 iLas2 targeted laser illumination system (Cairn, Faversham, Kent, UK). Excitation light
533 was transmitted through either a quad dichroic beam splitter (TRF89902-QUAD) or a
534 dichroic mirror (for 425 nm; ZT442rdc-UF2) (Chroma). Emitted light was passed through
535 appropriate filters (Cairn Optospin; peak/bandwidth: 480/40, 525/50, 630/75 and
536 700/75 nm) and detected with an iXon Ultra 897 electron multiplied charge-coupled device
537 (EMCCD) camera (512 × 512 pixels, Andor). For TIRFM, the penetration depth was
538 100 nm. The iLas2 illumination system was used for TIRFM and wide-field imaging. For
539 experiments with RNb-Perceval-HR, a 150× oil-immersion TIRF objective (NA 1.45) and
540 a Prime 95B Scientific metal-oxide-semiconductor (CMOS) camera (512 × 512 pixels,
541 Photometrics) were used.

542 For CALI and LOV2/zdk1 experiments, the 488-nm laser in the upright position
543 delivered an output at the objective of 2.45 mW (PM100A power meter, Thor Labs,
544 Newton, NJ, USA). For CALI, a single flash of 488-nm laser illumination (3-s duration)
545 was applied, with 10-ms exposures to 488-nm laser immediately before and after the CALI
546 flash to allow imaging of SNAP-Cell-fluorescein (i.e. 3.02 s total CALI flash). For
547 LOV2/zdk1 experiments, repeated flashes of 488-nm light (1-s duration each) were used at
548 2-s intervals to allow imaging with 561-nm laser illumination during the intervening
549 periods.

550 Before analysis, all fluorescence images were corrected for background by subtraction
551 of fluorescence detected from a region outside the cell. Image capture and processing used
552 MetaMorph Microscopy Automation and Image Analysis Software (Molecular Devices)
553 and Fiji [95]. Particle tracking used the TrackMate ImageJ plugin [96], with an estimated
554 blob diameter of 17 pixels and a threshold of 5 pixels. Co-localization analysis used the
555 JACoP ImageJ plugin [97]. Pearson's correlation coefficient (r) was used to quantify
556 colocalization. We report r values only when the Costes' randomization-based colocalization
557 value (P-value = 100 after 100 iterations) confirmed the significance of the original
558 colocalization. Where example images are shown, they are representative of at least three
559 independent experiments (individual plates of cells from different transfections and days).

560

561 **Statistics**

562 Results are presented as mean \pm SEM for particle-tracking analyses and mean \pm SD for
563 colocalization analyses, from n independent analyses (individual plates of cells from
564 different transfections). Statistical comparisons used paired or unpaired Student's t -tests,
565 or analysis of variance with the Bonferroni correction used for multiple comparisons. * $p <$
566 0.05 was considered significant.

567

568 **Declarations**

569

570 **Availability of data and materials**

571 All plasmids and data generated or analysed during this study are included in this published
572 article and its supplementary information files. Plasmids are available from the corresponding
573 authors on request and from Addgene.

574

575 **Competing interests**

576 The authors confirm that they have no competing interests.

577

578 **Funding**

579 This work was supported by the Biotechnology and Biological Sciences Research Council
580 UK (grant number BB/P005330/1) and a Wellcome Trust Senior Investigator Award (grant
581 number 101844).

582

583 **Authors' contributions**

584 DLP and CWT conceived the work. DLP conducted all experiments and analysis. DLP and
585 CWT interpreted data and wrote the manuscript. DLP and CWT read and approved the final
586 manuscript.

587

588 **Acknowledgements**

589 Not applicable.

590

591

592 **Ethics Approval and Consent to Participate**

593 Not applicable

594

595 **References**

- 596 1. Clift D, McEwan WA, Labzin LI, Konieczny V, Mogessie B, James LC, et al. A
597 method for the acute and rapid degradation of endogenous proteins. *Cell*.
598 2018;171:1692-706.e18.
- 599 2. Helma J, Cardoso MC, Muyldermans S, Leonhardt H. Nanobodies and recombinant
600 binders in cell biology. *J Cell Biol*. 2015;209:633-44.
- 601 3. Shaner NC, Steinbach PA, Tsien RY. A guide to choosing fluorescent proteins. *Nat*
602 *Methods*. 2005;2:905-9.
- 603 4. Rodriguez EA, Campbell RE, Lin JY, Lin MZ, Miyawaki A, Palmer AE, et al. The
604 growing and glowing toolbox of fluorescent and photoactive proteins. *Trends Biochem*
605 *Sci*. 2017;42:111-29.
- 606 5. Leonetti MD, Sekine S, Kamiyama D, Weissman JS, Huang B. A scalable strategy for
607 high-throughput GFP tagging of endogenous human proteins. *Proc Natl Acad Sci USA*.
608 2016;113:E3501-8.
- 609 6. Stewart-Ornstein J, Lahav G. Dynamics of CDKN1A in single cells defined by an
610 endogenous fluorescent tagging toolkit. *Cell Rep*. 2016;14:1800-11.
- 611 7. Thillaiappan NB, Chavda AP, Tovey SC, Prole DL, Taylor CW. Ca²⁺ signals initiate at
612 immobile IP₃ receptors adjacent to ER-plasma membrane junctions. *Nat Commun*.
613 2017;8:1505.
- 614 8. Zhang J. The colorful journey of green fluorescent protein. *ACS Chem Biol*. 2009;4:85-
615 8.

- 616 9. Stadler C, Rexhepaj E, Singan VR, Murphy RF, Pepperkok R, Uhlen M, et al.
617 Immunofluorescence and fluorescent-protein tagging show high correlation for protein
618 localization in mammalian cells. *Nat Methods*. 2013;10:315-23.
- 619 10. Hein MY, Hubner NC, Poser I, Cox J, Nagaraj N, Toyoda Y, et al. A human
620 interactome in three quantitative dimensions organized by stoichiometries and
621 abundances. *Cell*. 2015;163:712-23.
- 622 11. Nagarkar-Jaiswal S, Lee PT, Campbell ME, Chen K, Anguiano-Zarate S, Gutierrez
623 MC, et al. A library of MiMICs allows tagging of genes and reversible, spatial and
624 temporal knockdown of proteins in *Drosophila*. *eLife*. 2015;4:e05338.
- 625 12. Huh WK, Falvo JV, Gerke LC, Carroll AS, Howson RW, Weissman JS, et al. Global
626 analysis of protein localization in budding yeast. *Nature*. 2003;425:686-91.
- 627 13. Hayashi A, Ding DQ, Tsutsumi C, Chikashige Y, Masuda H, Haraguchi T, et al.
628 Localization of gene products using a chromosomally tagged GFP-fusion library in the
629 fission yeast *Schizosaccharomyces pombe*. *Genes Cells*. 2009;14:217-25.
- 630 14. Yofe I, Weill U, Meurer M, Chuartzman S, Zalckvar E, Goldman O, et al. One library
631 to make them all: streamlining the creation of yeast libraries via a SWAp-Tag strategy.
632 *Nat Methods*. 2016;13:371-8.
- 633 15. Koroleva OA, Tomlinson ML, Leader D, Shaw P, Doonan JH. High-throughput protein
634 localization in *Arabidopsis* using *Agrobacterium*-mediated transient expression of GFP-
635 ORF fusions. *Plant J*. 2005;41:162-74.
- 636 16. Tian GW, Mohanty A, Chary SN, Li S, Paap B, Drakakaki G, et al. High-throughput
637 fluorescent tagging of full-length *Arabidopsis* gene products in planta. *Plant Physiol*.
638 2004;135:25-38.
- 639 17. Kitagawa M, Ara T, Arifuzzaman M, Ioka-Nakamichi T, Inamoto E, Toyonaga H, et al.
640 Complete set of ORF clones of *Escherichia coli* ASKA library (a complete set of *E.*

- 641 *coli* K-12 ORF archive): unique resources for biological research. DNA Res.
642 2005;12:291-9.
- 643 18. Eason MG, Damry AM, Chica RA. Structure-guided rational design of red fluorescent
644 proteins: towards designer genetically-encoded fluorophores. Curr Opin Struct Biol.
645 2017;45:91-9.
- 646 19. Harikumar A, Edupuganti RR, Sorek M, Azad GK, Markoulaki S, Sehnalova P, et al.
647 An endogenously tagged fluorescent fusion protein library in mouse embryonic stem
648 cells. Stem Cell Rep. 2017;9:1304-14.
- 649 20. Pollithy A, Romer T, Lang C, Muller FD, Helma J, Leonhardt H, et al. Magnetosome
650 expression of functional camelid antibody fragments (nanobodies) in *Magnetospirillum*
651 *gryphiswaldense*. Appl Environ Microbiol. 2011;77:6165-71.
- 652 21. Fridy PC, Li Y, Keegan S, Thompson MK, Nudelman I, Scheid JF, et al. A robust
653 pipeline for rapid production of versatile nanobody repertoires. Nat Methods.
654 2014;11:1253-60.
- 655 22. Rothbauer U, Zolghadr K, Muyldermans S, Schepers A, Cardoso MC, Leonhardt H. A
656 versatile nanotrap for biochemical and functional studies with fluorescent fusion
657 proteins. Mol Cell Proteomics. 2008;7:282-9.
- 658 23. Kanner SA, Morgenstern T, Colecraft HM. Sculpting ion channel functional expression
659 with engineered ubiquitin ligases. eLife. 2017;6:e29744.
- 660 24. Caussin E, Kanca O, Affolter M. Fluorescent fusion protein knockout mediated by
661 anti-GFP nanobody. Nat Struct Mol Biol. 2011;19:117-21.
- 662 25. Borg S, Popp F, Hofmann J, Leonhardt H, Rothbauer U, Schuler D. An intracellular
663 nanotrap redirects proteins and organelles in live bacteria. MBio. 2015;6:e02117.

- 664 26. Liu TK, Hsieh PY, Zhuang YD, Hsia CY, Huang CL, Lai HP, et al. A rapid SNAP-tag
665 fluorogenic probe based on an environment-sensitive fluorophore for no-wash live cell
666 imaging. *ACS Chem Biol.* 2014;9:2359-65.
- 667 27. Filadi R, Pozzan T. Generation and functions of second messengers microdomains. *Cell*
668 *Calcium.* 2015;58:405-14.
- 669 28. Ludwig FT, Schwab A, Stock C. The Na⁺/H⁺ -exchanger (NHE1) generates pH
670 nanodomains at focal adhesions. *J Cell Physiol.* 2012;228:1351-8.
- 671 29. Schlattner U, Klaus A, Ramirez Rios S, Guzun R, Kay L, Tokarska-Schlattner M.
672 Cellular compartmentation of energy metabolism: creatine kinase microcompartments
673 and recruitment of B-type creatine kinase to specific subcellular sites. *Amino Acids.*
674 2016;48:1751-74.
- 675 30. Zhao Y, Araki S, Wu J, Teramoto T, Chang YF, Nakano M, et al. An expanded palette
676 of genetically encoded Ca²⁺ indicators. *Science.* 2011;333:1888-91.
- 677 31. Sankaranarayanan S, De Angelis D, Rothman JE, Ryan TA. The use of pHluorins for
678 optical measurements of presynaptic activity. *Biophys J.* 2000;79:2199-208.
- 679 32. Shen Y, Rosendale M, Campbell RE, Perrais D. pHuji, a pH-sensitive red fluorescent
680 protein for imaging of exo- and endocytosis. *J Cell Biol.* 2014;207:419-32.
- 681 33. Tantama M, Martinez-Francois JR, Mongeon R, Yellen G. Imaging energy status in
682 live cells with a fluorescent biosensor of the intracellular ATP-to-ADP ratio. *Nat*
683 *Commun.* 2013;4:2550.
- 684 34. Atakpa P, Thillaiappan NB, Mataragka S, Prole DL, Taylor CW. IP₃ receptors
685 preferentially associate with ER-lysosome contact sites and selectively deliver Ca²⁺ to
686 lysosomes. *Cell Rep.* 2018;25:3180-93.

- 687 35. Mammucari C, Raffaello A, Vecellio Reane D, Gherardi G, De Mario A, Rizzuto R.
688 Mitochondrial calcium uptake in organ physiology: from molecular mechanism to
689 animal models. *Pflugers Arch.* 2018;470:1165-79.
- 690 36. Wang X, Schwarz TL. The mechanism of Ca^{2+} -dependent regulation of kinesin-
691 mediated mitochondrial motility. *Cell.* 2009;136:163-74.
- 692 37. Hajnóczky G, Robb-Gaspers LD, Seitz MB, Thomas AP. Decoding cytosolic calcium
693 oscillations in the mitochondria. *Cell.* 1995;82:415-24.
- 694 38. Giacomello M, Drago I, Bortolozzi M, Scorzeto M, Gianelle A, Pizzo P, et al. Ca^{2+} hot
695 spots on the mitochondrial surface are generated by Ca^{2+} mobilization from stores, but
696 not by activation of store-operated Ca^{2+} channels. *Mol Cell.* 2010;38:280-90.
- 697 39. Cole NB. Site-specific protein labeling with SNAP-tags. *Curr Prot Prot Sci.*
698 2014;73:Unit 30.1.
- 699 40. Ries J, Kaplan C, Platonova E, Eghlidi H, Ewers H. A simple, versatile method for
700 GFP-based super-resolution microscopy via nanobodies. *Nat Methods.* 2012;9:582-4.
- 701 41. Bodor DL, Rodriguez MG, Moreno N, Jansen LE. Analysis of protein turnover by
702 quantitative SNAP-based pulse-chase imaging. *Curr Prot Cell Biol.* 2012:Unit 8.
- 703 42. Sano Y, Watanabe W, Matsunaga S. Chromophore-assisted laser inactivation - towards
704 a spatiotemporal-functional analysis of proteins, and the ablation of chromatin,
705 organelle and cell function. *J Cell Sci.* 2014;127:1621-9.
- 706 43. Bonifacino JS, Neefjes J. Moving and positioning the endolysosomal system. *Curr*
707 *Opin Cell Biol.* 2017;47:1-8.
- 708 44. Lee S, Park H, Kyung T, Kim NY, Kim S, Kim J, et al. Reversible protein inactivation
709 by optogenetic trapping in cells. *Nat Methods.* 2014;11:633-6.
- 710 45. Robinson MS, Sahlender DA, Foster SD. Rapid inactivation of proteins by rapamycin-
711 induced rerouting to mitochondria. *Dev Cell.* 2010;18:324-31.

- 712 46. Wang H, Vilela M, Winkler A, Tarnawski M, Schlichting I, Yumerefendi H, et al.
713 LOVTRAP: an optogenetic system for photoinduced protein dissociation. *Nat Methods*.
714 2016;13:755-8.
- 715 47. Csordas G, Weaver D, Hajnoczky G. Endoplasmic reticular-mitochondrial
716 contactology: structure and signaling functions. *Trends Cell Biol*. 2018;28:523-40.
- 717 48. Csordas G, Varnai P, Golenar T, Roy S, Purkins G, Schneider TG, et al. Imaging
718 interorganelle contacts and local calcium dynamics at the ER-mitochondrial interface.
719 *Mol Cell*. 2010;39:121-32.
- 720 49. Tepikin AV. Mitochondrial junctions with cellular organelles: Ca²⁺ signalling
721 perspective. *Pflugers Arch*. 2018;470:1181-92.
- 722 50. Kennedy HJ, Pouli AE, Ainscow EK, Jouaville LS, Rizzuto R, Rutter GA. Glucose
723 generates sub-plasma membrane ATP microdomains in single islet beta-cells. Potential
724 role for strategically located mitochondria. *J Biol Chem*. 1999;274:13281-91.
- 725 51. Quintana A, Pasche M, Junker C, Al-Ansary D, Rieger H, Kummerow C, et al. Calcium
726 microdomains at the immunological synapse: how ORAI channels, mitochondria and
727 calcium pumps generate local calcium signals for efficient T-cell activation. *EMBO J*.
728 2011;30:3895-912.
- 729 52. Frieden M, Arnaudeau S, Castelbou C, Demaurex N. Subplasmalemmal mitochondria
730 modulate the activity of plasma membrane Ca²⁺-ATPases. *J Biol Chem*.
731 2005;280:43198-208.
- 732 53. Balla T. Ca²⁺ and lipid signals hold hands at endoplasmic reticulum-plasma membrane
733 contact sites. *J Physiol*. 2017;596:2709-16.
- 734 54. Prakriya M, Lewis RS. Store-operated calcium channels. *Physiol Rev*. 2015;95:1383-
735 436.

- 736 55. Chang CL, Hsieh TS, Yang TT, Rothberg KG, Azizoglu DB, Volk E, et al. Feedback
737 regulation of receptor-induced Ca^{2+} signaling mediated by E-Syt1 and Nir2 at
738 endoplasmic reticulum-plasma membrane junctions. *Cell Rep.* 2013;5:813-25.
- 739 56. Simmen T, Tagaya M. Organelle communication at membrane contact sites (MCS):
740 from curiosity to center stage in cell biology and biomedical research. *Adv Exp Med*
741 *Biol.* 2017;997:1-12.
- 742 57. Wong YC, Ysselstein D, Krainc D. Mitochondria-lysosome contacts regulate
743 mitochondrial fission via RAB7 GTP hydrolysis. *Nature.* 2017;554:382-6.
- 744 58. Torres S, Balboa E, Zanlungo S, Enrich C, Garcia-Ruiz C, Fernandez-Checa JC.
745 Lysosomal and mitochondrial liaisons in Niemann-Pick disease. *Front Physiol.*
746 2017;8:982.
- 747 59. Wu J, Prole DL, Shen Y, Lin Z, Gnanasekaran A, Liu Y, et al. Red fluorescent
748 genetically encoded Ca^{2+} indicators for use in mitochondria and endoplasmic reticulum.
749 *Biochem J.* 2014;464:13-22.
- 750 60. Suzuki J, Kanemaru K, Ishii K, Ohkura M, Okubo Y, Iino M. Imaging intraorganellar
751 Ca^{2+} at subcellular resolution using CEPIA. *Nat Commun.* 2014;5:4153.
- 752 61. Suzuki J, Kanemaru K, Iino M. Genetically encoded fluorescent indicators for
753 organellar calcium imaging. *Biophys J.* 2016;111:1119-31.
- 754 62. Hirabayashi Y, Kwon SK, Paek H, Pernice WM, Paul MA, Lee J, et al. ER-
755 mitochondria tethering by PDZD8 regulates Ca^{2+} dynamics in mammalian neurons.
756 *Science.* 2017;358:623-30.
- 757 63. Konieczny V, Tovey SC, Mataragka S, Prole DL, Taylor CW. Cyclic AMP recruits a
758 discrete intracellular Ca^{2+} store by unmasking hypersensitive IP_3 receptors. *Cell Rep.*
759 2017;18:711-22.

- 760 64. Rodriguez-Prados M, Rojo-Ruiz J, Aulestia FJ, Garcia-Sancho J, Alonso MT. A new
761 low-Ca²⁺ affinity GAP indicator to monitor high Ca²⁺ in organelles by luminescence.
762 Cell Calcium. 2015;58:558-64.
- 763 65. Konieczny V, Keebler MV, Taylor CW. Spatial organization of intracellular Ca²⁺
764 signals. Semin Cell Dev Biol. 2012;23:172-80.
- 765 66. Langeberg LK, Scott JD. Signalling scaffolds and local organization of cellular
766 behaviour. Nat Rev Mol Cell Biol. 2015;16:232-44.
- 767 67. Ariotti N, Rae J, Giles N, Martel N, Sierceki E, Gambin Y, et al. Ultrastructural
768 localisation of protein interactions using conditionally stable nanobodies. PLoS Biol.
769 2018;16:e2005473.
- 770 68. Rost BR, Schneider-Warme F, Schmitz D, Hegemann P. Optogenetic tools for
771 subcellular applications in neuroscience. Neuron. 2017;96:572-603.
- 772 69. Ruggiu AA, Bannwarth M, Johnsson K. Fura-2FF-based calcium indicator for protein
773 labeling. Org Biomol Chem. 2010;8:3398-401.
- 774 70. Kamiya M, Johnsson K. Localizable and highly sensitive calcium indicator based on a
775 BODIPY fluorophore. Anal Chem. 2010;82:6472-9.
- 776 71. Bannwarth M, Correa IR, Sztretye M, Pouvreau S, Fellay C, Aebischer A, et al. Indo-1
777 derivatives for local calcium sensing. ACS Chem Biol. 2009;4:179-90.
- 778 72. Wang C, Song X, Xiao Y. SNAP-tag-based subcellular protein labeling and fluorescent
779 imaging with naphthalimides. ChemBioChem. 2017;18:1762-9.
- 780 73. Abo M, Minakami R, Miyano K, Kamiya M, Nagano T, Urano Y, et al. Visualization
781 of phagosomal hydrogen peroxide production by a novel fluorescent probe that is
782 localized via SNAP-tag labeling. Anal Chem. 2014;86:5983-90.

- 783 74. Zimmermann M, Cal R, Janett E, Hoffmann V, Bochet CG, Constable E, et al. Cell-
784 permeant and photocleavable chemical inducer of dimerization. *Angew Chem Int Ed*
785 *Engl.* 2014;53:4717-20.
- 786 75. Feng S, Laketa V, Stein F, Rutkowska A, MacNamara A, Depner S, et al. A rapidly
787 reversible chemical dimerizer system to study lipid signaling in living cells. *Angew*
788 *Chem Int Ed Engl.* 2014;53:6720-3.
- 789 76. Putyrski M, Schultz C. Protein translocation as a tool: The current rapamycin story.
790 *FEBS Lett.* 2012;586:2097-105.
- 791 77. Marschall AL, Dubel S, Boldicke T. Specific in vivo knockdown of protein function by
792 intrabodies. *MAbs.* 2015;7:1010-35.
- 793 78. Michelangeli F, Ogunbayo OA, Wootton LL. A plethora of interacting organellar Ca^{2+}
794 stores. *Curr Opin Cell Biol.* 2005;17:135-40.
- 795 79. Wong AK, Capitanio P, Lissandron V, Bortolozzi M, Pozzan T, Pizzo P. Heterogeneity
796 of Ca^{2+} handling among and within Golgi compartments. *J Mol Cell Biol.* 2013;5:266-
797 76.
- 798 80. Crevenna AH, Blank B, Maiser A, Emin D, Prescher J, Beck G, et al. Secretory cargo
799 sorting by Ca^{2+} -dependent Cab45 oligomerization at the trans-Golgi network. *J Cell*
800 *Biol.* 2016;213:305-14.
- 801 81. Appenzeller C, Andersson H, Kappeler F, Hauri HP. The lectin ERGIC-53 is a cargo
802 transport receptor for glycoproteins. *Nat Cell Biol.* 1999;1:330-4.
- 803 82. Mitchell KJ, Pinton P, Varadi A, Tacchetti C, Ainscow EK, Pozzan T, et al. Dense core
804 secretory vesicles revealed as a dynamic Ca^{2+} store in neuroendocrine cells with a
805 vesicle-associated membrane protein aequorin indicator. *J Cell Biol.* 2001;155:41-51.
- 806 83. Mundorf ML, Troyer KP, Hochstetler SE, Near JA, Wightman RM. Vesicular Ca^{2+}
807 participates in the catalysis of exocytosis. *J Biol Chem.* 2000;275:9136-42.

- 808 84. Harmansa S, Affolter M. Protein binders and their applications in developmental
809 biology. *Development*. 2018;145:dev148874.
- 810 85. Tiede C, Bedford R, Heseltine SJ, Smith G, Wijetunga I, Ross R, et al. Affimer proteins
811 are versatile and renewable affinity reagents. *eLife*. 2017;6:e24903.
- 812 86. Sha F, Salzman G, Gupta A, Koide S. Monobodies and other synthetic binding proteins
813 for expanding protein science. *Protein Sci*. 2017;26:910-24.
- 814 87. Wozniak MJ, Bola B, Brownhill K, Yang YC, Levakova V, Allan VJ. Role of kinesin-1
815 and cytoplasmic dynein in endoplasmic reticulum movement in VERO cells. *J Cell Sci*.
816 2009;122:1979-89.
- 817 88. Lopez Sanjurjo CI, Tovey SC, Prole DL, Taylor CW. Lysosomes shape $\text{Ins}(1,4,5)\text{P}_3$ -
818 evoked Ca^{2+} signals by selectively sequestering Ca^{2+} released from the endoplasmic
819 reticulum. *J Cell Sci*. 2013;126:289-300.
- 820 89. Brailoiu E, Churamani D, Cai X, Schrlau MG, Brailoiu GC, Gao X, et al. Essential
821 requirement for two-pore channel 1 in NAADP-mediated calcium signaling. *J Cell*
822 *Biol*. 2009;186:201-19.
- 823 90. Kanda T, Sullivan KF, Wahl GM. Histone-GFP fusion protein enables sensitive
824 analysis of chromosome dynamics in living mammalian cells. *Curr Biol*. 1998;8:377-
825 85.
- 826 91. English AR, Voeltz GK. Rab10 GTPase regulates ER dynamics and morphology. *Nat*
827 *Cell Biol*. 2013;15:169-78.
- 828 92. Cheeseman LP, Harry EF, McAinsh AD, Prior IA, Royle SJ. Specific removal of
829 TACC3-ch-TOG-clathrin at metaphase deregulates kinetochore fiber tension. *J Cell*
830 *Sci*. 2013;126:2102-13.

- 831 93. Goedhart J, von Stetten D, Noirclerc-Savoye M, Lelimosin M, Joosen L, Hink MA, et
832 al. Structure-guided evolution of cyan fluorescent proteins towards a quantum yield of
833 93%. *Nat Commun.* 2012;3:751.
- 834 94. Violin JD, Ren XR, Lefkowitz RJ. G-protein-coupled receptor kinase specificity for β -
835 arrestin recruitment to the β_2 -adrenergic receptor revealed by fluorescence resonance
836 energy transfer. *J Biol Chem.* 2006;281:20577-88.
- 837 95. Schindelin J, Arganda-Carreras I, Frise E, Kaynig V, Longair M, Pietzsch T, et al. Fiji:
838 an open-source platform for biological-image analysis. *Nat Methods.* 2012;9:676-82.
- 839 96. Jaqaman K, Loerke D, Mettlen M, Kuwata H, Grinstein S, Schmid SL, et al. Robust
840 single-particle tracking in live-cell time-lapse sequences. *Nat Methods.* 2008;5:695-
841 702.
- 842 97. Bolte S, Cordelieres FP. A guided tour into subcellular colocalization analysis in light
843 microscopy. *J Microsc.* 2006;224:213-32.

844

845

846 **Fig 1. Nanobody fusions for visualizing and manipulating intracellular signalling.**

847 Plasmids were generated that encode nanobodies specific for GFP variants (GNb) or RFP
848 variants (RNb), fused to functional modules. Nanobody fusions with an N-terminal signal
849 sequence to target them to the secretory pathway are also shown (ss-GNb and ss-RNb).

850

851 **Fig 2. RNb and GNb fusion proteins bind to their respective tagged proteins in live cells.**

852 (A) Schematic of the RNb-GFP fusion binding to RFP. (B) HeLa cells expressing RNb-GFP
853 with RFP-tagged markers for the ER surface (mCh-Sec61 β), the mitochondrial surface
854 (TOM20-mCh), the nucleus (H2B-mCh) or the surface of lysosomes (TPC2-mRFP). Cells
855 were imaged in HBS using epifluorescence microscopy (cells expressing H2B-mCh) or
856 TIRFM (other cells). Yellow boxes indicate regions enlarged in the subsequent panels.

857 Colocalization values (Pearson's coefficient, r) were: mCh-Sec61 β ($r = 0.93 \pm 0.09$, $n = 10$
858 cells); TOM20-mCh ($r = 0.94 \pm 0.09$, $n = 10$ cells); H2B-mCh ($r = 0.97 \pm 0.06$, $n = 10$ cells)
859 and TPC2-mRFP ($r = 0.78 \pm 0.09$, $n = 5$ cells). (C) Schematic of the GNb-mCh fusion

860 binding to GFP. (D) HeLa cells co-expressing GNb-mCh with GFP-tagged markers for the
861 ER surface (GFP-ERcyt), the mitochondrial surface (TOM20-GFP) and the nucleus (H2B-
862 GFP), or an mTurquoise2-tagged ER-surface marker (mTurq-ERcyt). Cells were imaged
863 using epifluorescence microscopy (cells expressing H2B-GFP) or TIRFM (other cells).

864 Yellow boxes indicate regions enlarged in the subsequent panels. Colocalization values were:
865 GFP-ERcyt ($r = 0.92 \pm 0.08$, $n = 8$ cells); TOM20-GFP ($r = 0.87 \pm 0.05$, $n = 7$ cells); H2B-
866 GFP ($r = 0.94 \pm 0.07$, $n = 6$ cells) and mTurq-ERcyt ($r = 0.97 \pm 0.03$, $n = 7$ cells). Scale bars
867 10 μm (main images) or 2.5 μm (enlargements).

868 **Fig 3. Targeting RNb-Ca²⁺ sensors to RFP-tagged proteins.** (A) Schematic of RNb-
869 GGECO fusion binding to RFP. (B-D) HeLa cells expressing RNb-GGECO1.2 and TOM20-
870 mCh, before and after addition of histamine (100 μ M) and then ionomycin (5 μ M). Cells
871 were imaged in HBS using TIRFM. The TOM20-mCh image is shown after the histamine
872 and ionomycin additions. The merged images are shown using images of RNb-GGECO1.2
873 after ionomycin (B, C) or histamine (D). The yellow and cyan boxed regions in panel B are
874 shown enlarged in panels C and D, respectively. Scale bars are 10 μ m (B) or 1.25 μ m (C, D).
875 (E) Timecourse of the effects of histamine (100 μ M) and ionomycin (5 μ M) on the
876 fluorescence of RNb-GGECO1.2 (F/F_0 , where F and F_0 are fluorescence recorded at t and $t =$
877 0). The traces are from regions coinciding with a single mitochondrion or cytosol (regions
878 identified in panel D), indicating changes in $[Ca^{2+}]$ at the OMM. (F) Enlarged region (70-180
879 s) of the graph shown in E. Results are representative of cells from 13 independent
880 experiments.

881 **Fig 4. Targeted GNB-Ca²⁺ sensors detect changes in [Ca²⁺] at the surface of**
882 **mitochondria.** (A) Schematic of GNB-RGECO fusion binding to GFP. (B, C) Representative
883 HeLa cells co-expressing TOM20-GFP and GNB-RGECO1.2 imaged in HBS using TIRFM
884 before and after addition of histamine (100 μ M) and then ionomycin (5 μ M). The TOM20-
885 GFP images are shown after the histamine and ionomycin additions. Histamine and
886 ionomycin evoked changes in fluorescence of GNB-RGECO1.2 at the OMM. The yellow
887 boxed region in panel B is shown enlarged in panel C. (D-F) Similar analyses of HeLa cells
888 co-expressing TOM20-GFP and GNB-LAR-GECO1.2 (GNB-LARG1.2). Histamine (100 μ M)
889 evoked changes in fluorescence of GNB-LARG1.2 at the OMM of mitochondria in the
890 perinuclear region (region of interest 1 (ROI 1) in E), but not in a peripheral region (ROI 2 in
891 F). All mitochondria responded to ionomycin (5 μ M), indicating that histamine evoked local
892 changes in [Ca²⁺] at the OMM. The cyan and yellow boxed regions in D are shown enlarged
893 in E and F, respectively. Scale bars 10 μ m (B, D) or 2.5 μ m (C, E, F). (G) Timecourse of the
894 changes in fluorescence of GNB-RGECO1.2 at the OMM evoked by histamine and
895 ionomycin for the entire cell shown in B. (H) Fluorescence changes recorded from ROI 1 and
896 ROI 2 in panels E and F. Results are representative of cells from 4 independent experiments.

897 **Fig 5. Targeting H⁺ sensors to RFP-tagged and GFP-tagged proteins.** (A) Schematic of
898 RNb fused to the pH sensor superecliptic pHluorin (RNb-SEpH) and bound to RFP. (B)
899 Schematic of GNB-pHuji binding to RFP. (C, D) HeLa cells co-expressing RNb-SEpH and
900 TOM20-mCh were imaged in modified HBS (MHBS) using epifluorescence microscopy and
901 exposed to extracellular pH 6.5 (C) or pH 8 (D) in the presence of nigericin (10 μ M). Scale
902 bars 10 μ m. (E, F) HeLa cells co-expressing GNB-pHuji and TOM20-GFP were exposed to
903 extracellular pH 6.5 (E) or pH 8 (F) in the presence of nigericin. Scale bars 10 μ m. (G, H)
904 Timecourse from single cells of the fluorescence changes (F/F_0) of mitochondrially targeted
905 RNb-SEpH or GNB-pHuji evoked by the indicated manipulations of extracellular pH. Results
906 shown are representative of 3 independent experiments.

907

908 **Fig 6. Targeting an ATP/ADP sensor to RFP-tagged proteins.** (A) Schematic of RNb-
909 Perceval-HR fusion (RNb-PHR) bound to RFP. (B) HeLa cells co-expressing RNb-PHR and
910 TOM20-mCh were imaged in HBS using epifluorescence microscopy. The yellow box
911 indicates the region enlarged in subsequent panels. Scale bars 10 μ m (main image) and 2.5
912 μ m (enlarged images). (C, D) Changes in fluorescence for each excitation wavelength (405
913 and 488 nm, F/F_0) (C) and their ratio (R/R_0 , where $R = F_{405}/F_{488}$) (D) of mitochondrially
914 targeted RNb-Perceval-HR after addition of 2-deoxyglucose (2DG, 10 mM), oligomycin
915 (OM, 1 μ M) and antimycin (AM, 1 μ M). The results indicate a decrease in the ATP/ADP
916 ratio at the OMM. Results are representative of 3 independent experiments.

917 **Fig 7. Nanobody-SNAPf fusion proteins allow labelling of RFP-tagged and GFP-tagged**
918 **proteins with fluorescent O⁶-benzylguanine derivatives in live cells. (A, B) Schematics of**
919 **RNb-SNAPf fusion bound to RFP, and GNb-SNAPf fusion bound to GFP, after labelling with**
920 **SNAP-Cell-647-SiR (magenta circles). (C-F) HeLa cells co-expressing RNb-SNAPf and**
921 **mitochondrial TOM20-mCh (C), RNb-SNAPf and lysosomal LAMP1-mCh (D), GNb-**
922 **SNAPf and TOM20-GFP (E) or GNb-SNAPf and LAMP1-GFP (F) were treated with SNAP-**
923 **Cell-647-SiR (0.5 μ M, 30 min at 37°C) and imaged using TIRFM. Scale bars 10 μ m (main**
924 **images) or 2.5 μ m (enlarged images of yellow boxed regions). Colocalization values: RNb-**
925 **SNAPf + TOM20-mCh ($r = 0.95 \pm 0.02$, $n = 6$ cells); RNb-SNAPf + LAMP1-mCh ($r = 0.84$**
926 **± 0.06 , $n = 8$ cells); GNb-SNAPf + TOM20-GFP ($r = 0.78 \pm 0.09$, $n = 10$ cells); and GNb-**
927 **SNAPf + LAMP1-GFP ($r = 0.85 \pm 0.10$, $n = 11$ cells).**

928 **Fig 8. Targeting CALI to lysosomes using RNb-SNAPf reduces lysosomal motility. (A)**
929 Schematic of RNb-SNAPf after labelling with SNAP-Cell-fluorescein (green circle) and
930 bound to RFP. **(B)** HeLa cells co-expressing LAMP1-mCh and RNb-SNAPf were incubated
931 with SNAP-Cell-fluorescein (0.5 μ M, 30 min, 37°C), which labelled lysosomes
932 (colocalization values, $r = 0.73 \pm 0.02$, $n = 6$ cells), and imaged using TIRFM. **(C, D)** Cells
933 were then exposed to 488-nm light for 3 s to induce CALI. TIRFM images show a
934 representative cell at different times before **(C)** and after **(D)** CALI, with the image at $t = 0$ s
935 shown in magenta and the image at $t = 60$ s in green. White in the merged images from the
936 two different times indicates immobile lysosomes, while green and magenta indicate
937 lysosomes that moved in the interval between images. Yellow boxes show regions enlarged in
938 subsequent images. Scale bars 10 μ m (main images) and 2.5 μ m (enlargements). For clarity,
939 images were auto-adjusted for brightness and contrast (ImageJ) to compensate for bleaching
940 of mCh during tracking and CALI. **(E)** Effect of CALI on the displacements of individual
941 lysosomes, determining by particle-tracking (TrackMate), during a 60-s recording from a
942 representative cell (images taken every 1 s; mean values shown by bars). **(F)** Summary data
943 (mean \pm SEM, $n = 6$ cells from 6 independent experiments) show the mean fractional
944 decrease in displacement (Δ Displacement) due to CALI in cells expressing RNb-SNAPf or
945 cytosolic SNAPf (see *Additional file 1: Fig. S2*). The fractional decrease in displacement for
946 each cell was defined as: $(MD_{pre} - MD_{post}) / MD_{pre}$, where MD_{pre} and MD_{post} are the mean
947 displacement of all tracked particles in 60 s before and after CALI. * $p < 0.05$, unpaired
948 Student's t -test.

949 **Fig 9. Clustering of RFP-tagged and GFP-tagged proteins and organelles using RNb-**
950 **mCerulean-MP and GNb-mRFP-MP.** (A) Schematic of RNb-mCerulean-MP fusion bound
951 to RFP. (B) Schematic of GNb-mRFP-MP fusion bound to GFP. (C-F) HeLa cells expressing
952 RFP-tagged proteins in the absence (C, E) or presence (D, F) of co-expressed RNb-
953 mCerulean-MP (RNb-mCer-MP) were imaged using epifluorescence microscopy. (G-N)
954 HeLa cells expressing GFP-tagged proteins in the absence (G, I, K, M) or presence (H, J, L,
955 N) of co-expressed GNb-mRFP-MP were imaged using epifluorescence microscopy. Results
956 are representative of at least 5 cells, from at least 3 independent experiments. Scale bars 10
957 μm .

958 **Fig 10. RNb-FKBP inducibly recruits ER transmembrane proteins to mitochondria. (A)**
959 Schematic of RNb-FKBP bound to RFP. **(B)** Schematic of GNb-FKBP bound to GFP. **(C, D)**
960 HeLa cells co-expressing RNb-FKBP, mitochondrial TOM70-GFP-FRB and mCh-Sec61 β
961 were imaged using TIRFM. A representative cell ($n = 7$) is shown before **(C)** and after **(D)**
962 treatment with rapamycin (100 nM, 10 min). The boxed region is enlarged in subsequent
963 images. Scale bars 10 μm (main images) and 2.5 μm (enlargements). **(E)** Timecourse of
964 mCh-Sec61 β fluorescence changes (F/F_0) evoked by rapamycin recorded at a representative
965 mitochondrion and in nearby reticular ER. Results show ~80% loss of fluorescence from the
966 ER devoid of mitochondrial contacts. **(F, G)** HeLa cells co-expressing endogenously tagged
967 GFP-IP $_3$ R1, GNb-FKBP and mitochondrial TOM70-mCh-FRB were imaged using TIRFM. A
968 representative cell ($n = 6$) is shown before **(F)** and after **(G)** treatment with rapamycin (100
969 nM, 10 min). The boxed region is enlarged in subsequent images. Scale bars 10 μm (main
970 images) and 2.5 μm (enlargements). **(H)** HeLa cells co-expressing GFP-calmodulin (GFP-
971 CaM), GNb-FKBP and TOM20-mCh-FRB were imaged using epifluorescence microscopy. A
972 representative cell ($n = 3$) is shown before and after treatment with rapamycin (100 nM, 10
973 min). The image for TOM-mCh-FRB is shown in the presence of rapamycin. Scale bar 10
974 μm .

975 **Fig 11. Reversible optogenetic recruitment of RFP-tagged proteins using RNb-zdk1. (A)**

976 Schematic of RNb-zdk1 fusion bound to RFP, showing the reversible light-evoked
977 dissociation of zdk1 from LOV2. **(B)** HeLa cells co-expressing RNb-zdk1, mitochondrial
978 TOM20-LOV2 and cytosolic mCh were imaged using TIRFM. A representative cell is shown
979 before and after one or five 1-s exposures to blue light (488-nm laser at 2-s intervals) and
980 after a 3-min recovery period in the dark. Scale bar 10 μ m. **(C)** Timecourse of the mCherry
981 fluorescence changes (F/F_0) recorded at a representative mitochondrion and in nearby cytosol
982 after each of the indicated light flashes. There is a reversible decrease ($\sim 60\%$) in
983 mitochondrial mCh fluorescence and a corresponding reversible increase ($\sim 70\%$) in cytosolic
984 fluorescence. A single measurement of mCh fluorescence was made at the end of a 3-min
985 recovery period in the dark (REC) before further light flashes. Results are representative of 5
986 cells from 3 independent experiments.

987

988 **Fig 12. Recruitment of proteins to native PM-mitochondria MCS using RNb-FKBP. (A)**

989 Schematic of RNb-FKBP fusion bound to RFP. **(B, C)** HeLa cells co-expressing RNb-FKBP,
990 mitochondrial TOM70-GFP-FRB and β_2 AR-mCh were imaged using TIRFM before **(B)** and
991 after **(C)** treatment with rapamycin (100 nM, 10 min). Scale bar 10 μ m. **(D, E)** Enlarged
992 images from **C** of the yellow box **(D)** and cyan box **(E)** show punctate recruitment of β_2 AR-
993 mCh to individual mitochondria at the indicated times after addition of rapamycin. Scale bars
994 1.25 μ m. **(F)** TIRFM images of HeLa cells co-expressing mitochondrial TOM70-GFP-FRB
995 and β_2 AR-mCh in the presence of rapamycin (100 nM, 10 min) show no recruitment in the
996 absence of co-expressed RNb-FKBP. The yellow box shows a region enlarged in the
997 subsequent image. Scale bars 10 μ m (main images) and 2.5 μ m (enlargement). Results **(B-F)**
998 are representative of 5 independent experiments.

999 **Fig 13. Recruitment of PM proteins to ER-PM MCS using RNb-FKBP.** (A) Schematic of
1000 RNb-FKBP fusion bound to RFP. (B) HeLa cells co-expressing RNb-FKBP, mCh-Orai1 and
1001 the ER-PM junction marker GFP-MAPPER-FRB were imaged using TIRFM. A
1002 representative cell (n = 5) is shown before (top row) and after (bottom row) treatment with
1003 rapamycin (100 nM, 10 min). The boxed region is shown enlarged in subsequent images. (C)
1004 HeLa cells co-expressing mCh-Orai1 and GFP-MAPPER-FRB alone were imaged using
1005 TIRFM. A representative cell (n = 3) is shown before (top row) and after (bottom row)
1006 treatment with rapamycin (100 nM, 10 min). The boxed region is shown enlarged in
1007 subsequent images. The results show no recruitment in the absence of co-expressed RNb-
1008 FKBP. Scale bars (B, C) 10 μm (main images) and 2.5 μm (enlargements).

1009

1010 **Fig 14. Inducible recruitment of lysosomes to mitochondria using GNb-FKBP.** (A)
1011 Schematic of GNb-FKBP fusion bound to GFP. (B) HeLa cells co-expressing mitochondrial
1012 TOM70-mCh-FRB (magenta), lysosomal LAMP1-GFP (green) and GNb-FKBP were imaged
1013 using TIRFM. Merged images of a representative cell (n = 5) are shown before and at times
1014 after treatment with rapamycin (rapa, 100 nM). Scale bar 10 μm . (C) Enlargements of the
1015 boxed region in (B). Scale bar 2.5 μm . (D) HeLa cells co-expressing TOM70-mCh-FRB
1016 (magenta) and lysosomal LAMP1-GFP (green) were imaged using TIRFM. A representative
1017 cell (n = 3) is shown before and after treatment with rapamycin (100 μm , 10 min); there is no
1018 recruitment in the absence of co-expressed GNb-FKBP. The yellow box shows a region
1019 enlarged in the subsequent image. Scale bars 10 μm (main images) and 2.5 μm (enlargement).

1020 **Fig 15. Crosslinking GFP-tagged and RFP-tagged proteins and organelles using GNb-**
1021 **RNb.** (A) Schematic of GNb-RNb bound to GFP and RFP. (B-E) HeLa cells co-expressing
1022 the tagged proteins indicated with GNb-RNb were imaged using epifluorescence microscopy
1023 (B) or TIRFM (C-E). Representative cells (n = 5-7) are shown. Control images for GFP-
1024 IP₃R1 are shown in *Fig. 10* and *Additional file 1: Fig. S3*. (F, G) HeLa cells co-expressing
1025 LAMP1-GFP and LAMP1-mCh in the absence (F) or presence (G) of co-expressed GNb-
1026 RNb were imaged using TIRFM. Representative cells (n = 5) are shown. Scale bars (B-G) 10
1027 μm (main images) and 2.5 μm (enlargements of boxed areas).

1028

1029 **Fig 16. Inducible crosslinking of RFP-tagged and GFP-tagged proteins with GNb-FKBP**
1030 **and RNb-FRB.** (A) Schematic of the nanobody fusions used, with rapamycin shown as a
1031 blue sphere. (B, C) HeLa cells co-expressing GNb-FKBP, RNb-FRB, TOM20-GFP and mCh-
1032 Sec61β were imaged using TIRFM. A representative cell (n = 3) is shown before (B) and
1033 after (C) treatment with rapamycin (100 nM, 10 min). Scale bars 10 μm (main images) and
1034 2.5 μm (enlargements of boxed areas).

1035 **Fig 17. Nanobody fusions can be targeted to different luminal compartments of the**
1036 **secretory pathway. (A)** Schematic of ssGNb-mCh bound to GFP. **(B)** HeLa cells co-
1037 expressing ssGNb-mCh and either the luminal ER marker mTurquoise2-ERlumen, the
1038 marker of ER-PM junctions GFP-MAPPER, or the Golgi marker GFP-Golgi. Cells were
1039 imaged using epifluorescence microscopy. Representative cells are shown. Colocalization
1040 values were: mTurquoise2-ERlumen ($r = 0.96 \pm 0.03$, $n = 10$); GFP-MAPPER ($r = 0.94 \pm$
1041 0.02 , $n = 5$); and GFP-Golgi ($r = 0.91 \pm 0.06$, $n = 4$). **(C)** Schematic of ssRNb-GFP bound to
1042 RFP. **(D)** HeLa cells co-expressing ssRNb-GFP and either mCh-ERlumen or mCh-MAPPER
1043 were imaged using epifluorescence microscopy. Representative cells are shown.
1044 Colocalization values were: mCh-ERlumen ($r = 0.98 \pm 0.009$, $n = 9$) and mCh-MAPPER ($r =$
1045 0.93 ± 0.07 , $n = 13$. Scale bars 10 μm (main images) and 2.5 μm (enlargements of boxed
1046 regions).

1047 **Fig 18. Nanobody-mediated targeting of low-affinity Ca²⁺ sensors allows measurement**
1048 **of changes in [Ca²⁺] in an ER sub-compartment at ER-PM MCS. (A)** Schematic of
1049 ssRNb-Ca²⁺ sensor bound to RFP. **(B)** Schematic of ssGNb-Ca²⁺ sensor bound to GFP. **(C-F)**
1050 HeLa cells co-expressing the indicated combinations of mCh-MAPPER, GFP-MAPPER,
1051 ssRNb-GCEPIA (ssRNb-GC), ssRNb-GEMCEPIA (ssRNb-GEM; image is shown for the
1052 525-nm emission channel), ssGNb-LAR-GECO1 (ssGNb-LGECO) or ssGNb-RCEPIA were
1053 imaged in Ca²⁺-free HBS using TIRFM. Yellow boxes indicate regions enlarged in
1054 subsequent images. Scale bars 10 μm (main images) and 2.5 μm (enlargements). **(G-J)**
1055 Timecourses of fluorescence changes recorded from cells co-expressing mCh-MAPPER and
1056 ssRNb-GCEPIA (G), mCh-MAPPER and ssRNb-GEMCEPIA (H), GFP-MAPPER and
1057 ssGNb-LAR-GECO1 (ssGNb-LARG1) (I) and GFP-MAPPER and ssGNb-RCEPIA (J) in
1058 response to emptying of intracellular Ca²⁺ stores with ionomycin (5 μM). **(K)** Summary
1059 results (with mean ± SD, n = 4 cells) show fractional decreases (ΔF) in either fluorescence or
1060 emission ratio (for ssRNb-GEM) recorded 90 s after addition of ionomycin,

1061 **Additional files**

1062

1063 **Additional file 1 (.pptx):**

1064 **Figures S1-S6:** Fig. S1 - Targeting RNb-GEMGECO Ca²⁺ sensor to RFP-tagged proteins.

1065 Fig. S2 - Targeting CALI to lysosomes with SNAP-Cell-fluorescein: cytosolic controls. Fig.

1066 S3 - Rapamycin alone does not recruit RFP-tagged or GFP-tagged proteins to mitochondria.

1067 Fig. S4 - Recruitment of proteins to native PM-mitochondria MCS using GNb-FKBP.

1068 Fig. S5 - Inducible crosslinking of RFP-tagged and GFP-tagged proteins with RNb-FKBP

1069 and GNb-FRB. Fig. S6 - DNA sequences encoding the nanobodies used.

1070

1071 **Fig. S1 Targeting RNb-GEMGECO Ca²⁺ sensor to RFP-tagged proteins. (A)** Schematic

1072 of RNb-GEMGECO fusion binding to RFP. **(B)** HeLa cells co-expressing RNb-GEMGECO

1073 and TOM20-mCh were imaged in HBS using TIRFM. Images are shown before and after

1074 addition of histamine (100 μM) and then ionomycin (5 μM). The TOM20-mCh and merged

1075 images are before additions of histamine and ionomycin. The yellow boxed region in shown

1076 enlarged in (C). Scale bar 10 μm. **(C)** Enlarged regions from (B). Scale bar 2.5 μm. **(D, E)**

1077 Representative timecourses of histamine and ionomycin-evoked changes in fluorescence **(D)**

1078 and fluorescence emission ratio (R/R₀, where R = F₄₈₀/F₅₂₅) **(E)** of mitochondrially targeted

1079 RNb-GEMGECO. Results are representative of cells from 4 independent experiments.

1080 Relates to **Figs. 3 and 4.**

1081 **Fig. S2 Targeting CALI to lysosomes with SNAP-Cell-fluorescein: cytosolic controls. (A)**
1082 Schematic of cytosolic SNAPf, which does not bind to RFP, after its labelling with SNAP-
1083 Cell-fluorescein. **(B-D)** HeLa cells co-expressing LAMP1-mCh and cytosolic SNAPf (Cyt-
1084 SNAPf) were treated with SNAP-Cell-fluorescein (0.5 μ M, 30 min, 37°C) and imaged using
1085 TIRFM. Scale bar 10 μ m. Cells were then exposed to 488-nm light for 3 s to induce CALI.
1086 Images show a representative cell at different times before (C) and after (D) CALI, with the
1087 image at t = 0 s shown in magenta and the image at t = 60 s in green. White in the temporal
1088 merged image indicates immobile lysosomes, while green and magenta indicate lysosomes
1089 that moved during the 60 s between images. Yellow boxes show regions enlarged in
1090 subsequent images. Scale bars 10 μ m (main images) and 2.5 μ m (enlargements). For clarity,
1091 images were auto-adjusted for brightness and contrast (ImageJ) to compensate for bleaching
1092 of mCh during tracking and CALI. **(E)** Displacements of individual lysosomes during a 60-s
1093 recording (determined by TIRFM using TrackMate, with images taken every 1 s; mean values
1094 shown by bars) for a representative HeLa cell co-expressing LAMP1-mCh and cytosolic
1095 SNAPf before and after CALI (3-s exposure to 488-nm light). Typical of n = 6 cells.
1096 Summary data are shown in **Fig. 8F**. Relates to **Fig. 8**.

1097 **Fig. S3 Rapamycin alone does not recruit RFP-tagged or GFP-tagged proteins to**
1098 **mitochondria.** (A, B) HeLa cells co-expressing mitochondrial TOM70-mCh-FRB and mCh-
1099 Sec61 β were imaged using TIRFM before (A) and after (B) addition of rapamycin (100 nM,
1100 10 min). (C, D) HeLa cells co-expressing endogenously tagged GFP-IP₃R1 and
1101 mitochondrial TOM70-mCh-FRB were imaged using TIRFM before (C) and after (D)
1102 addition of rapamycin (100 nM, 10 min). (E) HeLa cells co-expressing GFP-calmodulin
1103 (GFP-CaM) and mitochondrial TOM70-mCh-FRB were imaged using TIRFM before and
1104 after addition of rapamycin (100 nM, 10 min). Results are each representative of cells from 3-
1105 5 independent experiments. Scale bars 10 μ m (main images) and 2.5 μ m (enlargements of
1106 boxed regions). Relates to **Fig. 10**.

1107

1108 **Fig. S4 Recruitment of proteins to native PM-mitochondria MCS using GNb-FKBP.** (A)
1109 Schematic of GNb-FKBP fusion bound to GFP. (B) TIRFM images of COS-7 cells co-
1110 expressing GNb-FKBP, β_2 AR-GFP and TOM70-mCh-FRB. A representative cell (n = 3) is
1111 shown before (top row) and at the indicated times after addition of rapamycin (100 nM).
1112 Scale bar 10 μ m. (C) Enlargements of the boxed regions in (B). Scale bar 3.75 μ m. Relates to
1113 **Fig. 12**.

1114

1115 **Fig. S5 Inducible crosslinking of RFP-tagged and GFP-tagged proteins with RNb-FKBP**
1116 **and GNb-FRB.** (A) Schematic of the nanobody fusions used, with rapamycin shown as a
1117 blue sphere. (B, C) HeLa cells co-expressing RNb-FKBP, GNb-FRB, TOM20-GFP and mCh-
1118 Sec61 β were imaged using TIRFM. A representative cell (n = 3) is shown before (B) and
1119 after (C) treatment with rapamycin (100 nM, 10 min). Scale bars 10 μ m (main images) and
1120 2.5 μ m (enlargements of boxed regions). Relates to **Fig. 16**.

1121

1122 **Fig. S6. DNA sequences encoding the nanobodies used.**

1123 **Additional file 2 (.wmv): Video 1. RNb-GGECO1.2 detects changes in $[Ca^{2+}]$ at the**
1124 **surface of mitochondria expressing TOM20-mCh.** The top panel shows RNb-GGECO1.2
1125 fluorescence (488-nm TIRFM excitation) and the bottom panel shows TOM20-mCh
1126 fluorescence (561-nm TIRFM excitation). In response to histamine (100 μ M, added at 60 s),
1127 local rises in $[Ca^{2+}]_c$ were detected at the surfaces of individual mitochondria, but not in the
1128 bulk cytosol. Ionomycin (5 μ M) was added at 3 min. Video was acquired at 1 Hz and is
1129 shown at 30 frames per second (fps). Clock is in min:s. Relates to **Fig. 3D**.

1130

1131 **Additional file 3 (.wmv): Video 2. GNb-LARGECO1.2 detects local changes in $[Ca^{2+}]$ at**
1132 **the surface of mitochondria expressing TOM20-GFP.** The video shows GNb-
1133 LARGECO1.2 fluorescence (488-nm TIRFM excitation). Histamine (100 μ M, added at 60 s)
1134 causes local rises in $[Ca^{2+}]_c$ at the OMM of individual mitochondria in the perinuclear region
1135 (cyan box in **Fig. 4D**), but not in peripheral regions (e.g. yellow box in **Fig. 4D**). Ionomycin
1136 (5 μ M) was added at 3 min. Video was acquired at 1 Hz and is shown at 33 fps. Clock is in
1137 min:s. Relates to **Fig. 4D-F**.

1138

1139 **Additional file 4 (.wmv): Video 3. Effect of targeted CALI on lysosomal motility.** HeLa
1140 cells expressing LAMP1-mCh and RNb-SNAPf were imaged using TIRFM and 561-nm laser
1141 illumination before (top) and after (bottom) CALI (3.02 s exposure to 488-nm
1142 epifluorescence laser illumination). Video was acquired at 0.5 Hz and is shown at 3 fps.
1143 Clock is in min:s. Relates to **Fig. 8**.

1144 **Additional file 5 (.wmv): Video 4. RNb-FKBP rapidly sequesters an ER integral**
1145 **membrane protein at the OMM.** TIRFM images of HeLa cells expressing TOM70-GFP-
1146 FRB, RNb-FKBP and mCh-Sec61 β were treated with rapamycin (100 nM, added at 60 s).
1147 The ER membrane protein, mCh-Sec61 β , is then rapidly sequestered at the OMM. Video was
1148 acquired at 0.5 Hz and shown at 33 fps. Clock is in min:s. Relates to *Fig. 10C* and *D*.

1149

1150 **Additional file 6 (.wmv): Video 5. GNb-FKBP rapidly sequesters endogenously tagged**
1151 **GFP-IP₃R1 at the OMM.** TIRFM images show HeLa cells with endogenously GFP-tagged
1152 IP₃R1 and transiently expressing TOM70-mCh-FRB and GNb-FKBP, and then treated with
1153 rapamycin (100 nM, added at 60 s). GFP-IP₃R1 is rapidly sequestered at the OMM. Video
1154 was acquired at 0.5 Hz and is shown at 33 fps. Clock is in min:s. Relates to *Fig. 10F* and *G*.

1155 .

1156 **Additional file 7 (.wmv): Video 6. GNb-FKBP rapidly sequesters GFP-CaM at the**
1157 **OMM.** Epifluorescence microscopy images show HeLa cells transiently expressing GFP-
1158 CaM, GNb-FKBP and TOM20-mCh-FRB, and then treated with rapamycin (100 nM, added
1159 at 30 s). GFP-CaM is rapidly sequestered at the OMM. Video was acquired at 0.5 Hz and is
1160 shown at 9 fps. Clock is in min:s. Relates to *Fig. 10H*.

1161

1162 **Additional file 8 (.wmv): Video 7. RNb-FKBP recruits a PM protein to the OMM in**
1163 **response to rapamycin.** TIRFM images of HeLa cells expressing TOM70-GFP-FRB, RNb-
1164 FKBP and the PM protein, β_2 AR-mCh, and then exposed to rapamycin (100 nM, added at 60
1165 s). There is a rapid translocation of β_2 AR-mCh to the OMM. Video was acquired at 0.5 Hz
1166 and is shown at 33 fps. Clock is in min:s. Relates to *Fig. 12B-E*.

1167

1168 **Additional file 9 (.wmv): Video 8. Crosslinking Gnb-FKBP and Rnb-FRB with**
1169 **rapamycin recruits mCh-Sec61 β to TOM20-GFP in the OMM.** HeLa cells expressing
1170 Gnb-FKBP, Rnb-FRB, mCh-Sec61 β and TOM20-GFP were stimulated with rapamycin
1171 (100 nM, added at 100 s). The TIRFM images show rapid recruitment of mCh-Sec61 β to the
1172 OMM. Video was acquired at 0.2 Hz and is shown at 8 fps. Clock is in min:s. Relates to **Fig.**
1173 **16.**

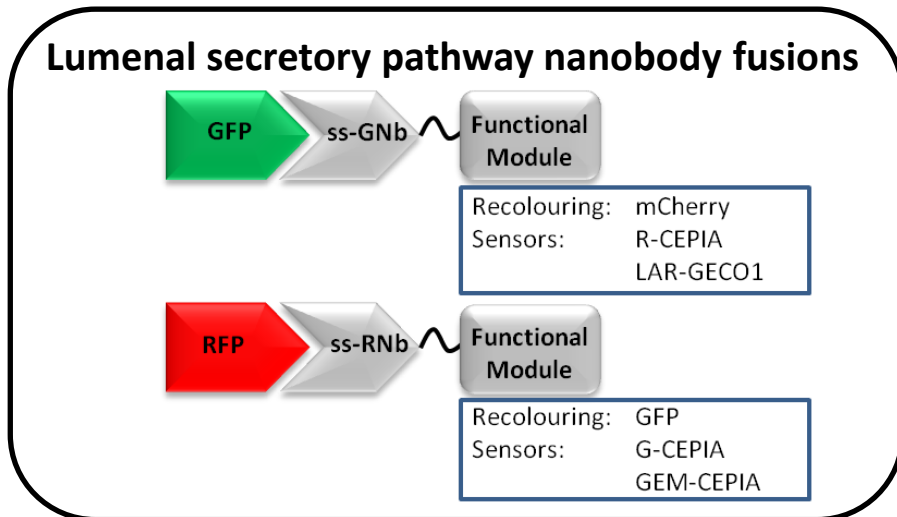
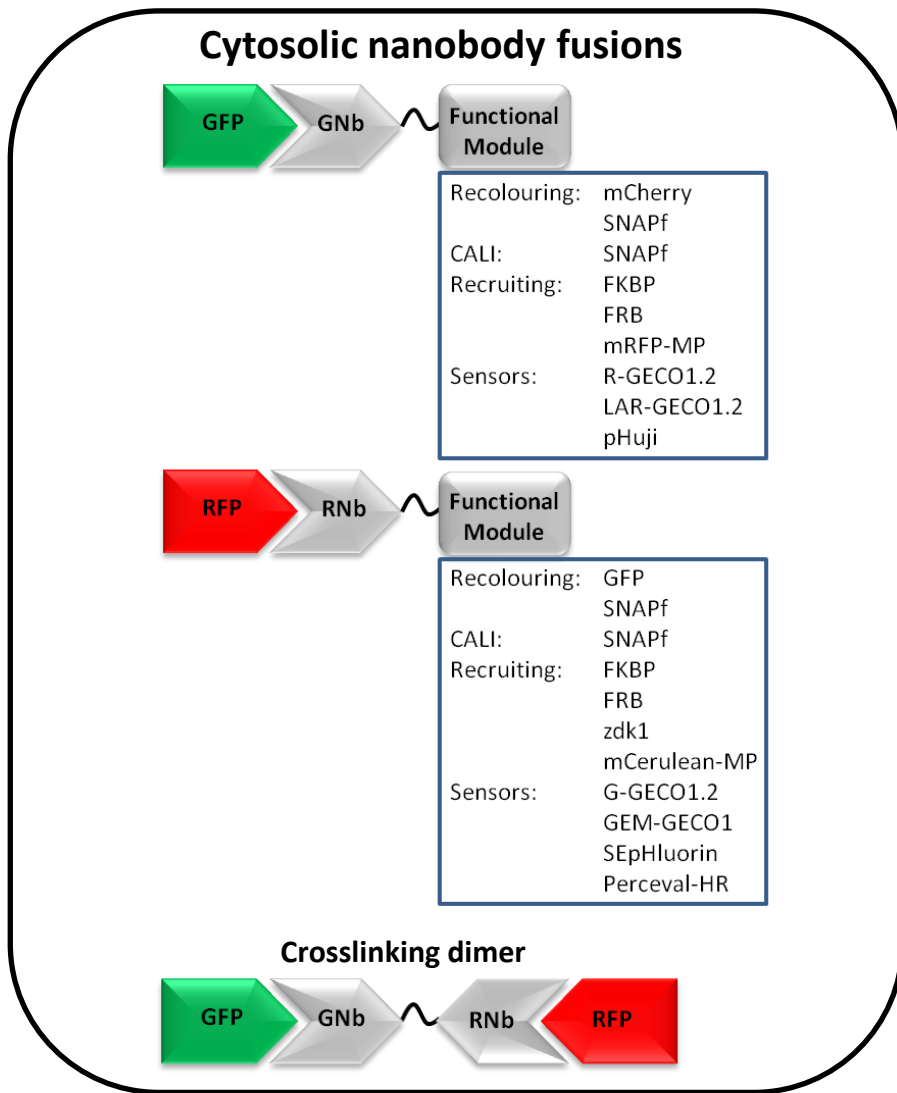


Figure 1.

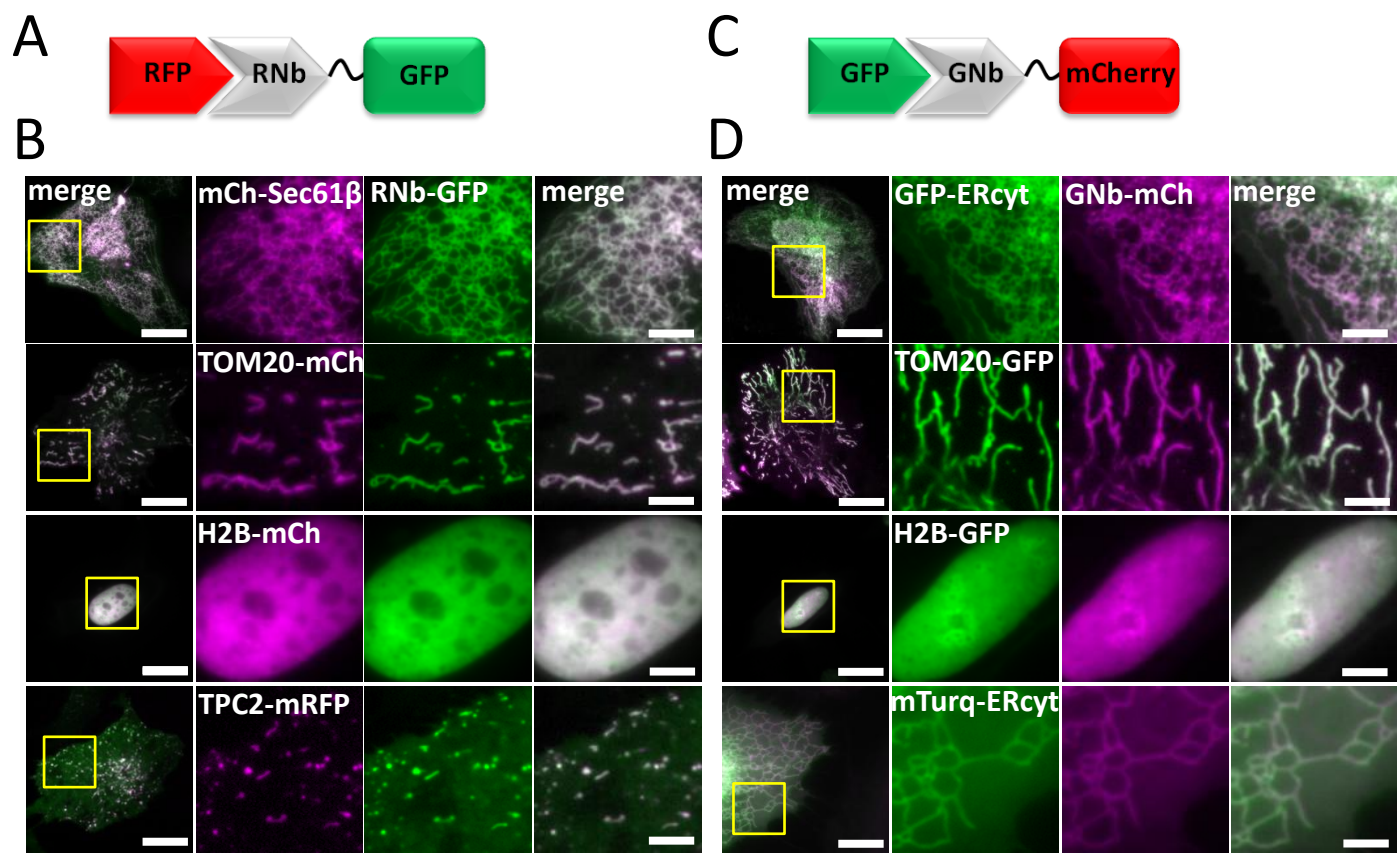


Figure 2.

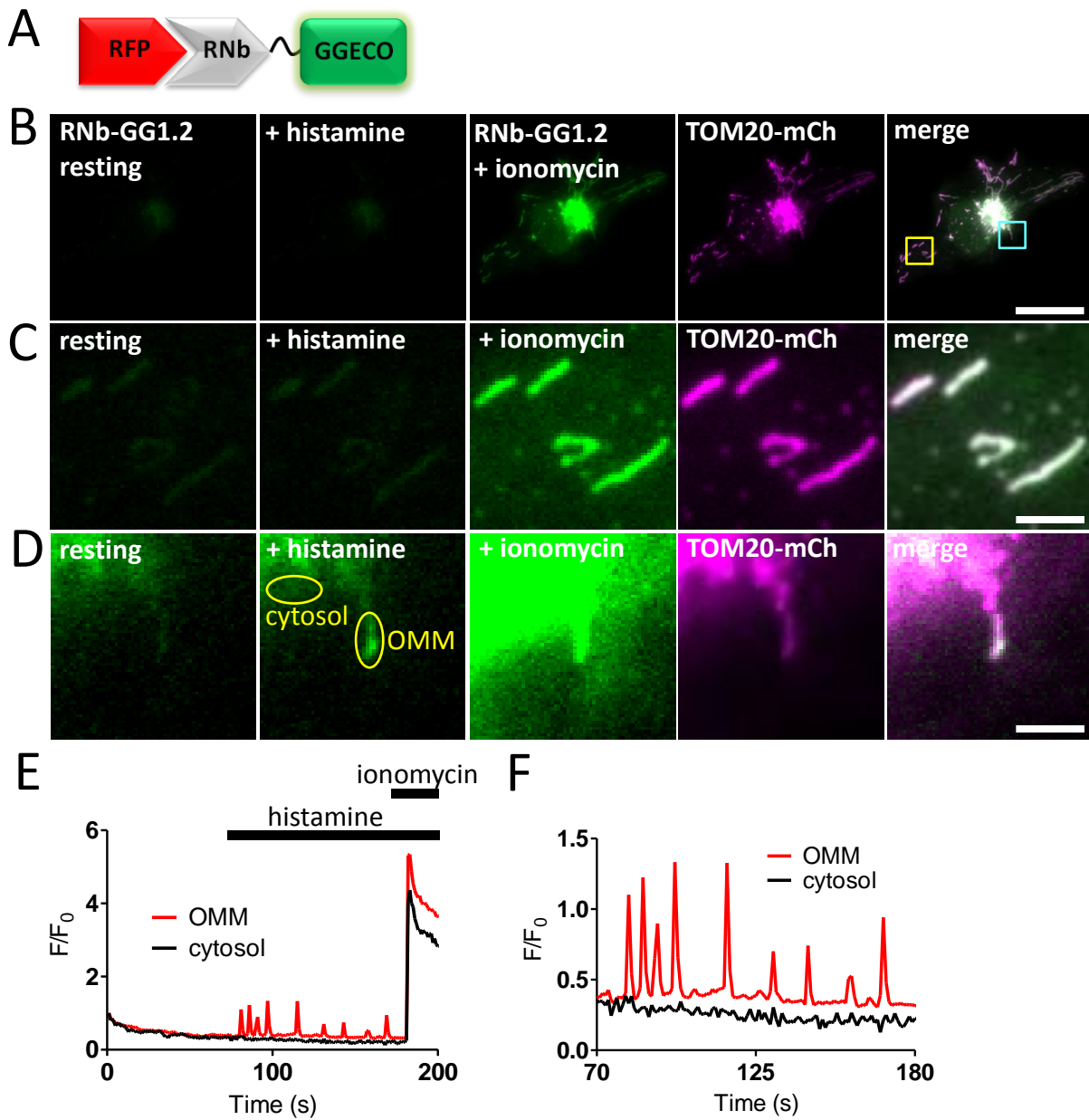


Figure 3.

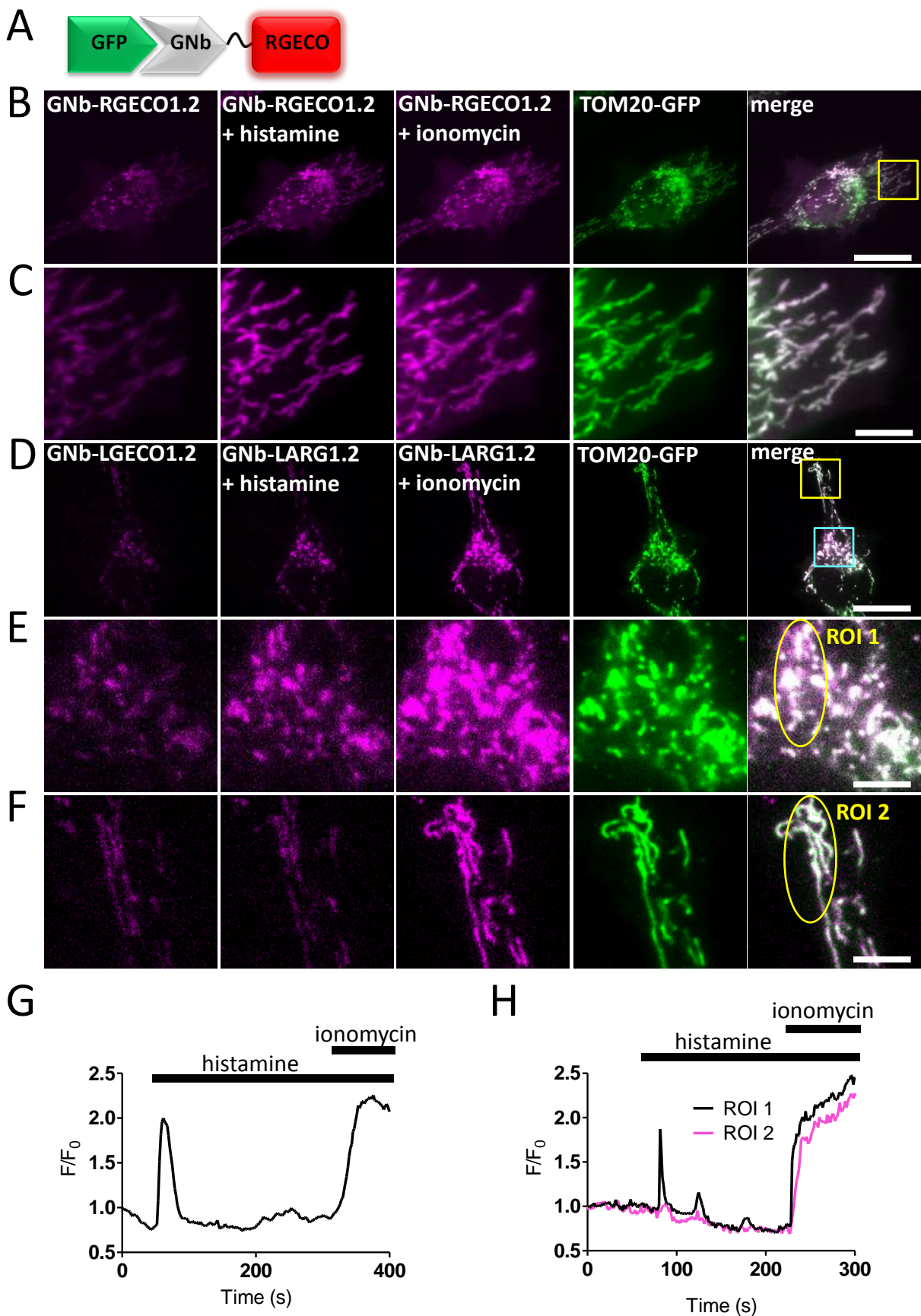


Figure 4.

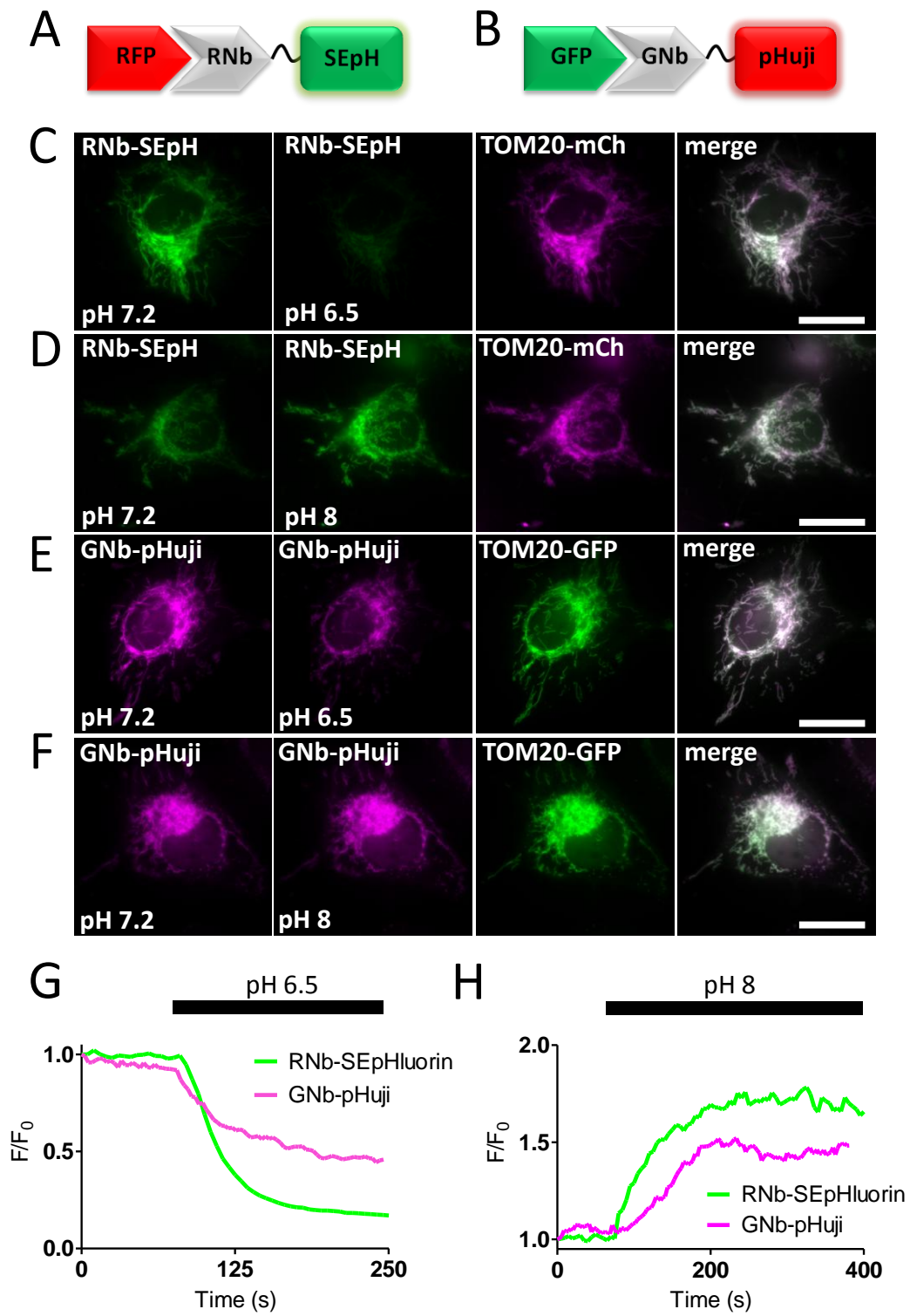


Figure 5.

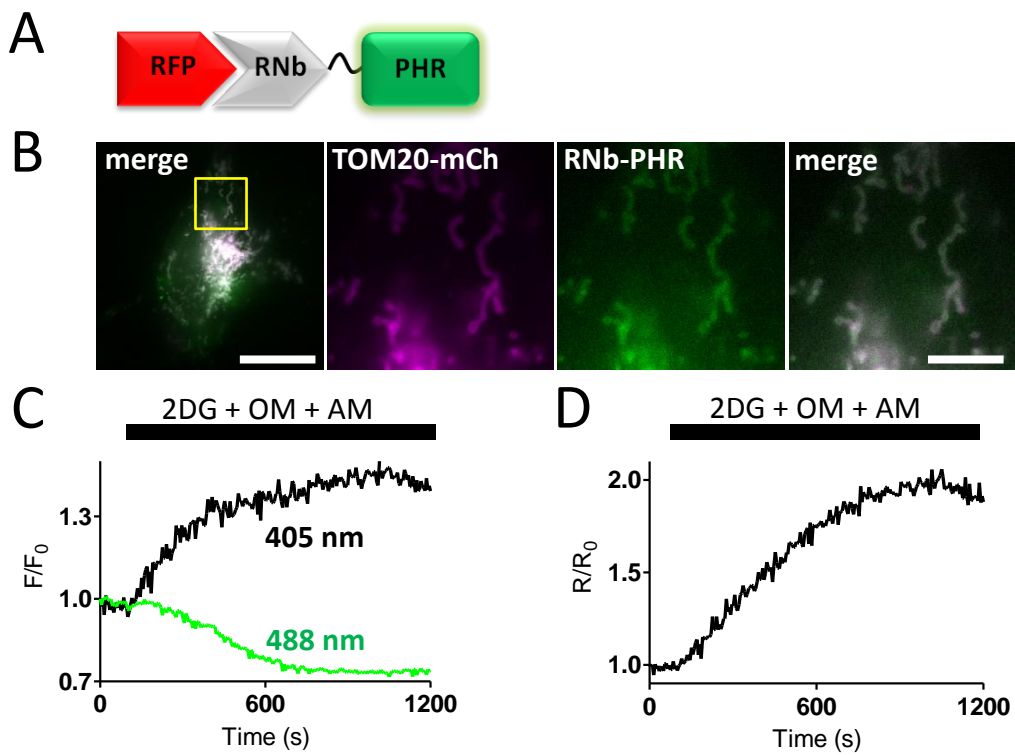


Figure 6.

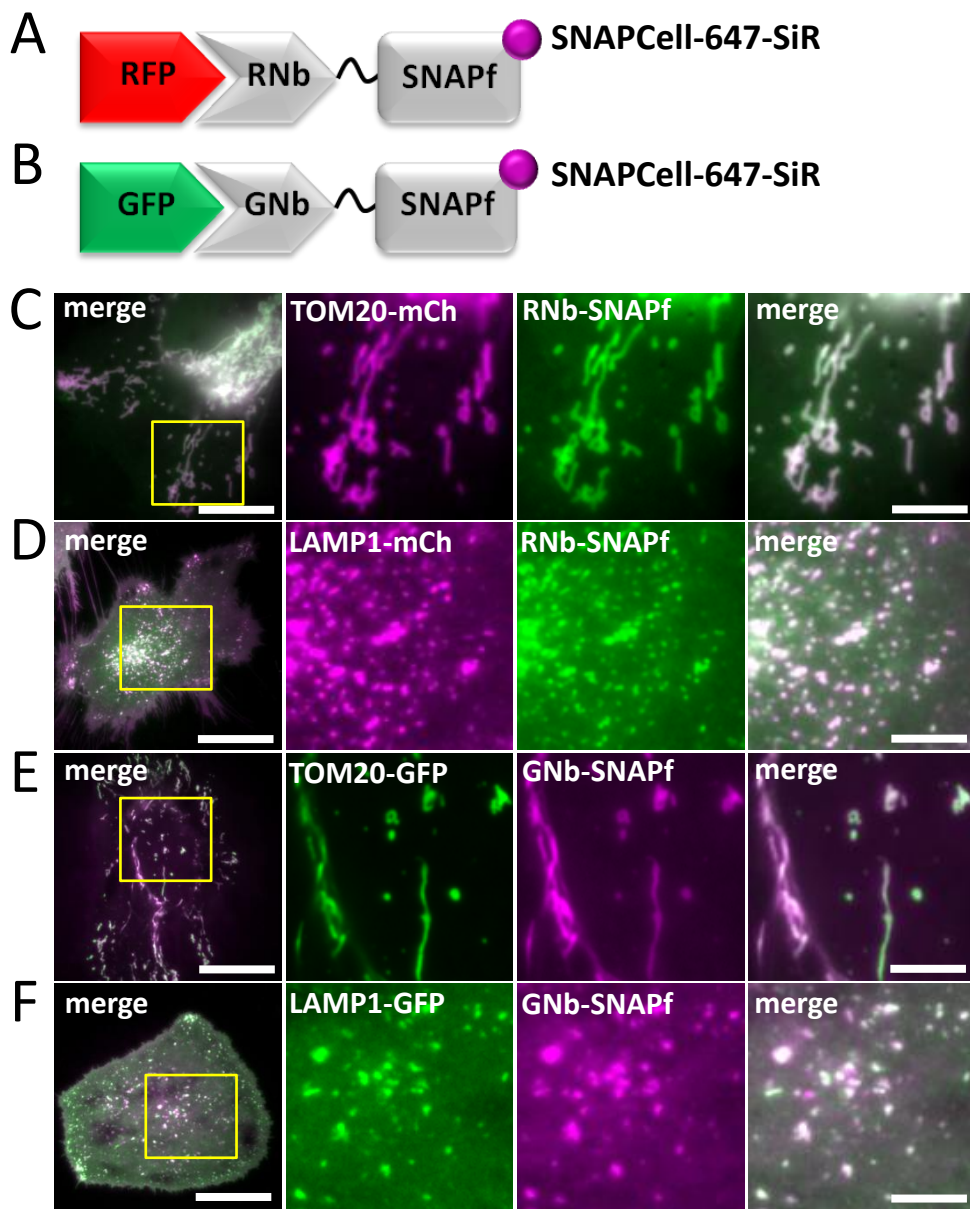


Figure 7.

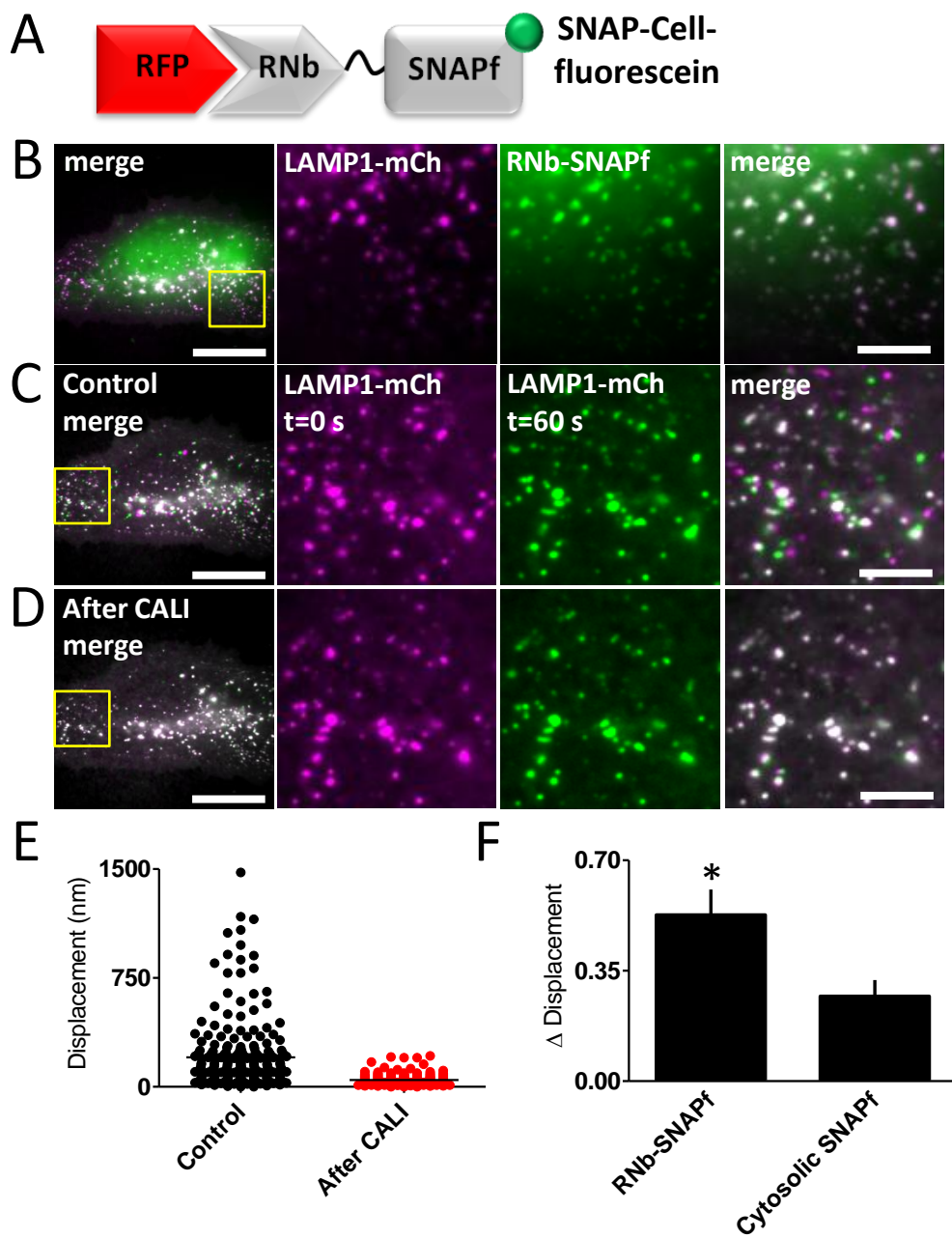


Figure 8.

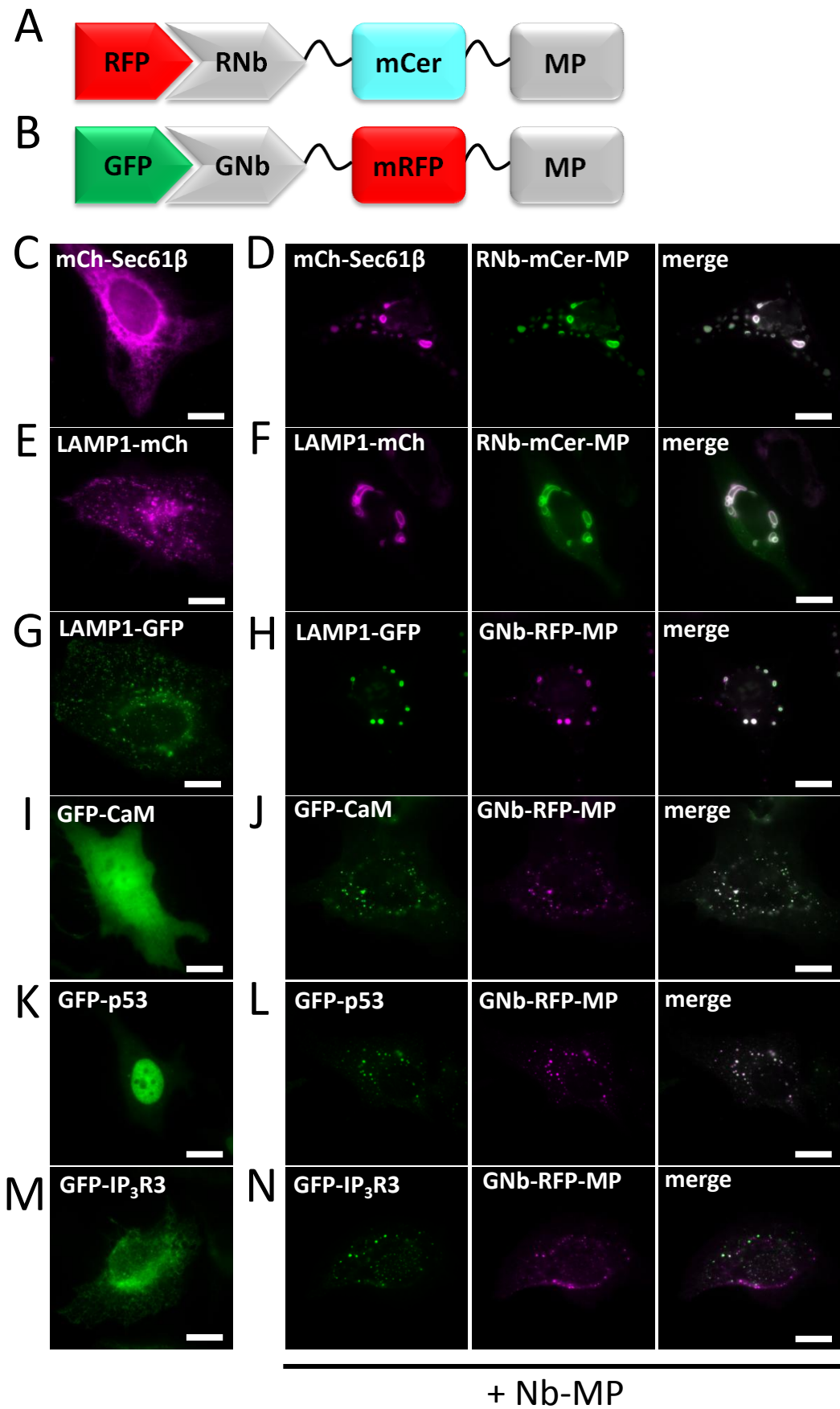


Figure 9.

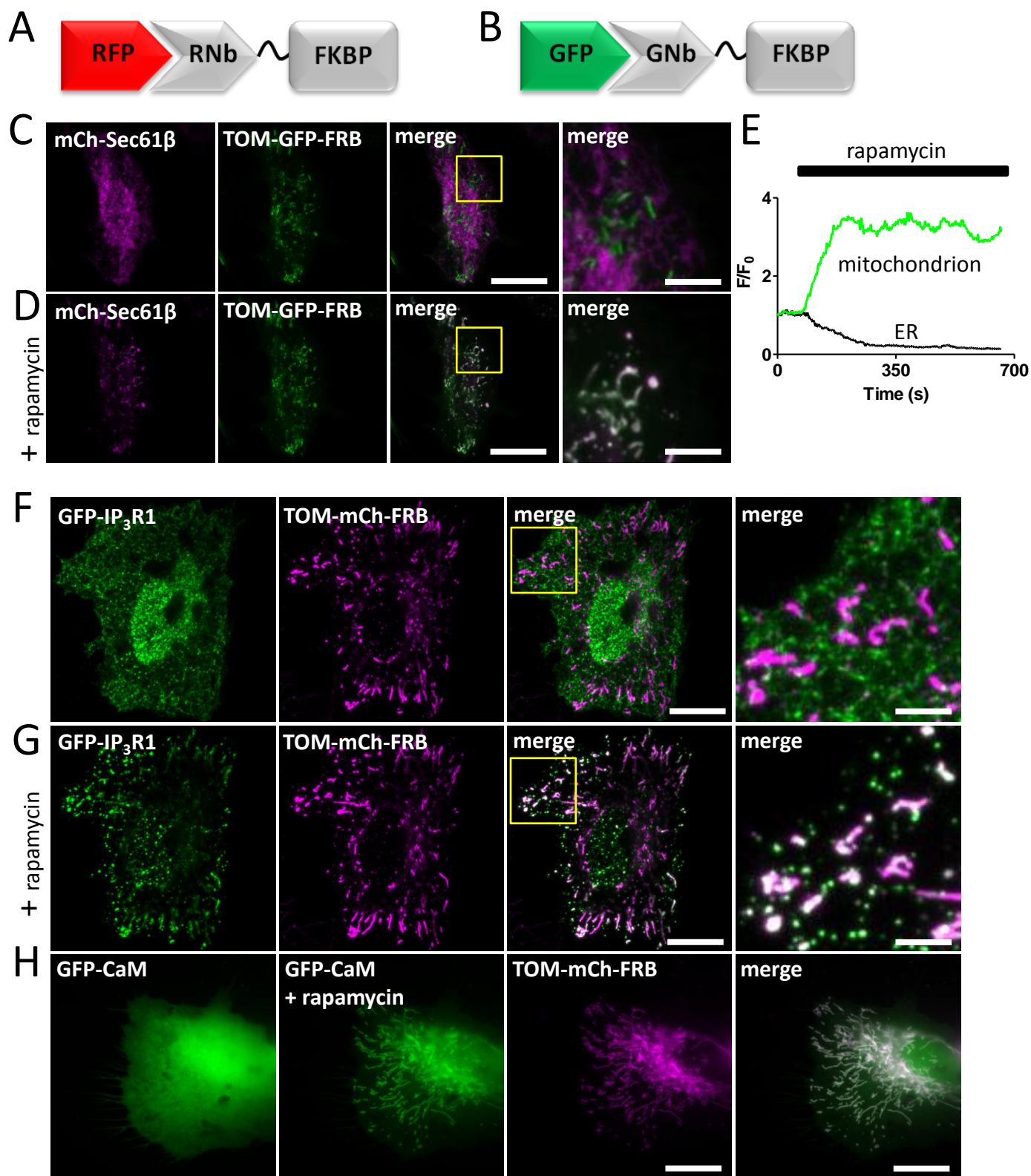


Figure 10.

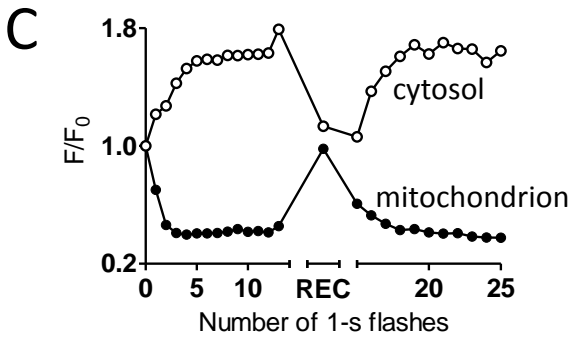
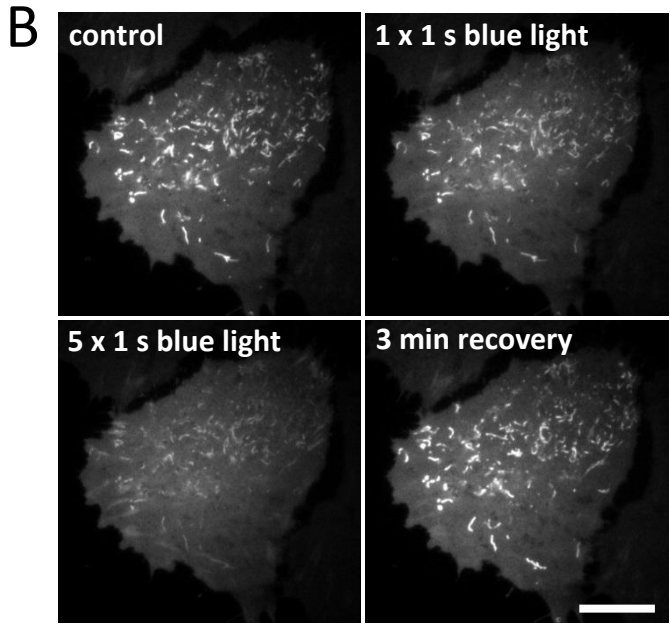
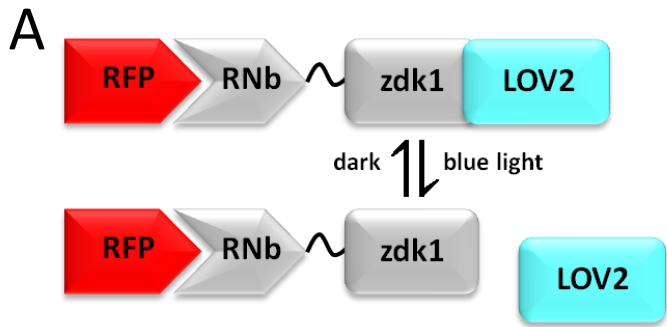


Figure 11.

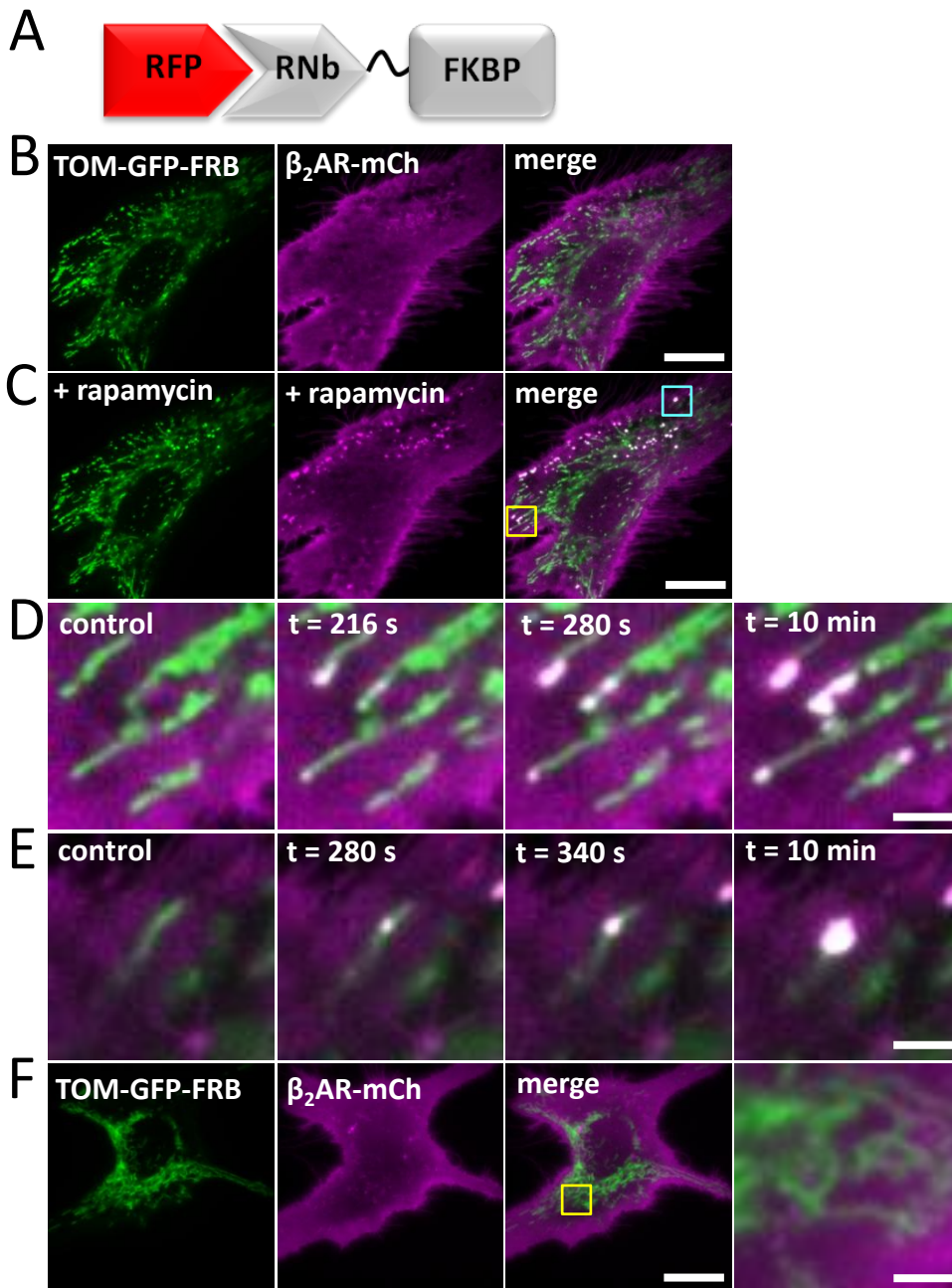


Figure 12.

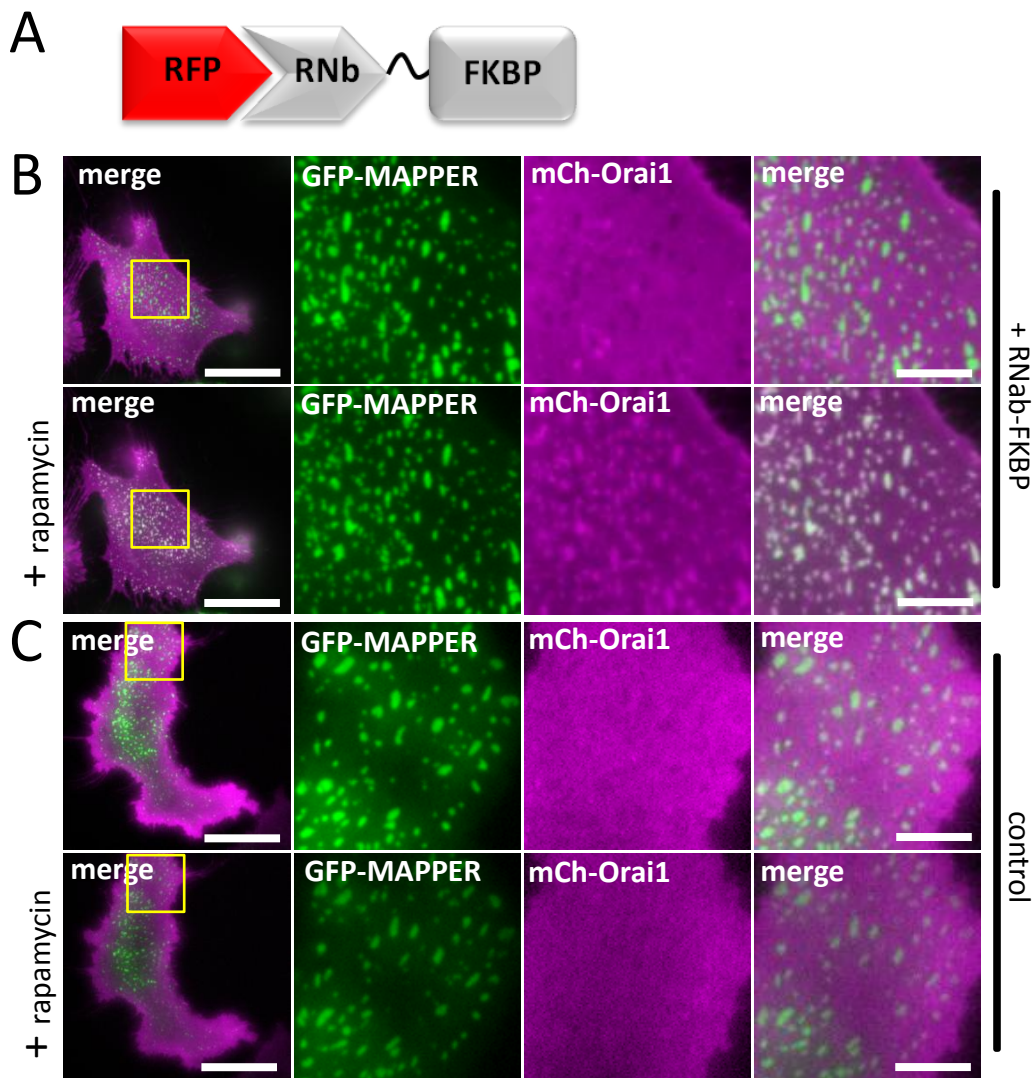


Figure 13.

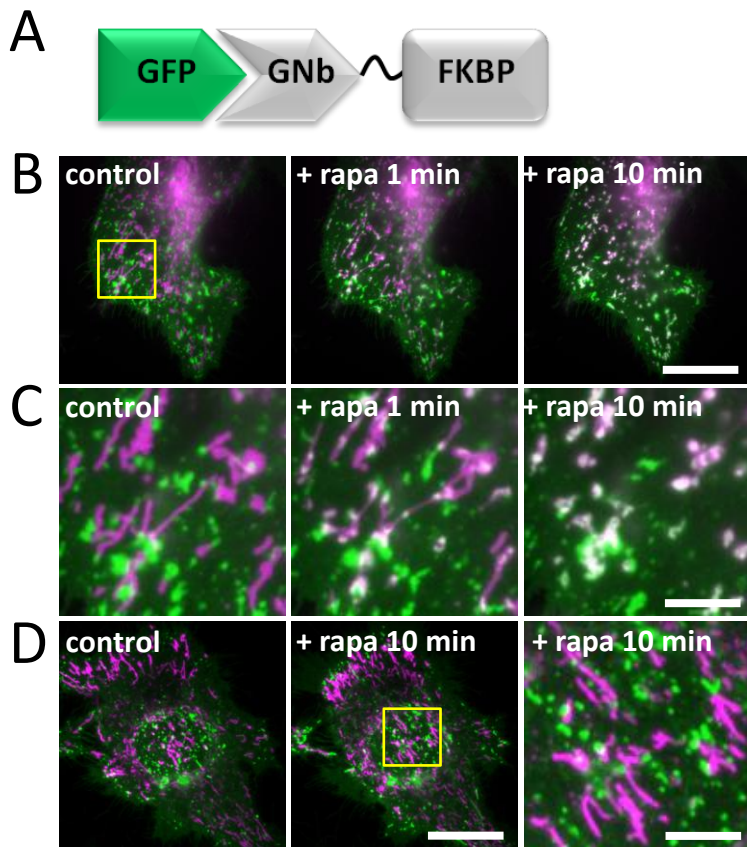


Figure 14.

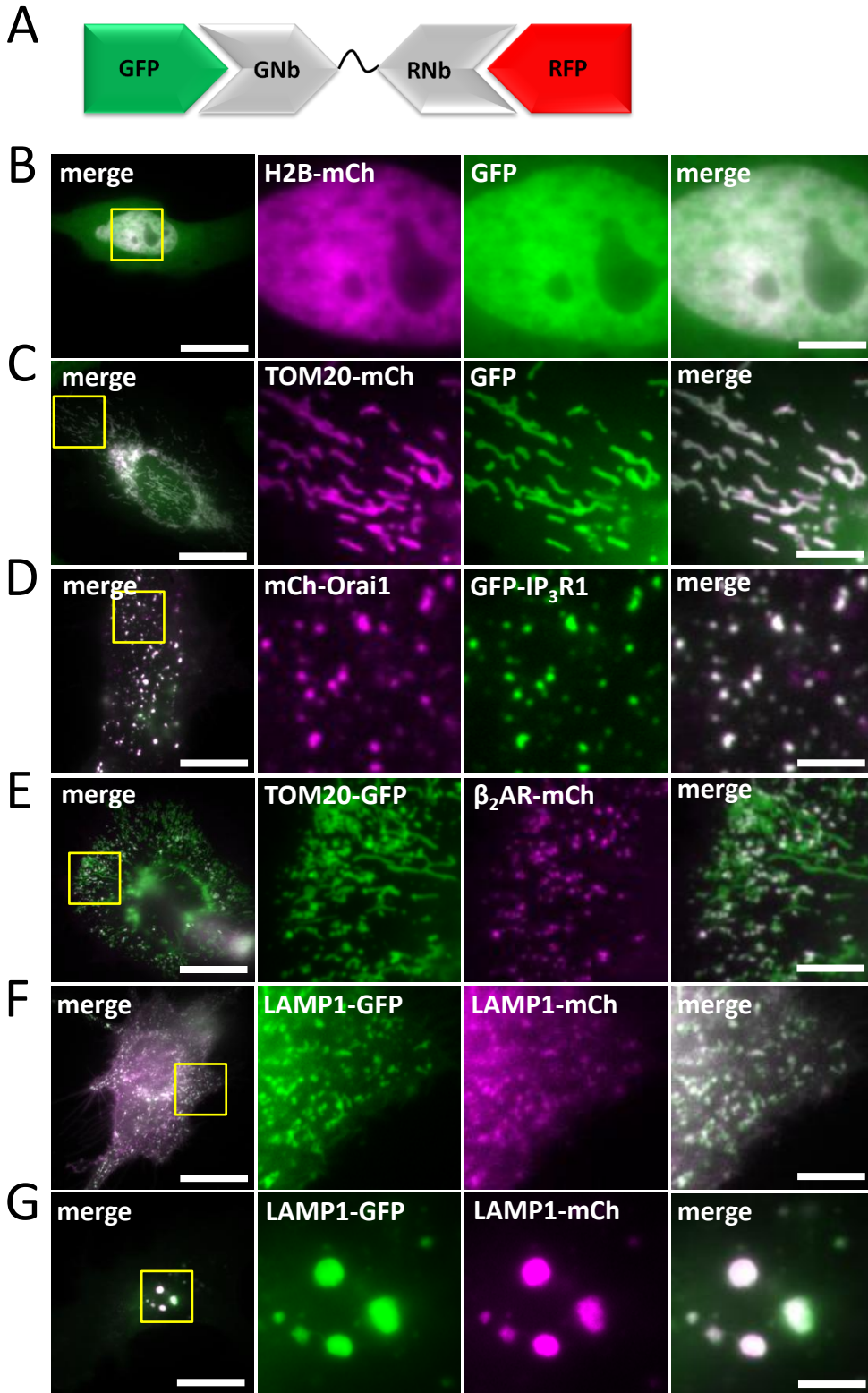


Figure 15.

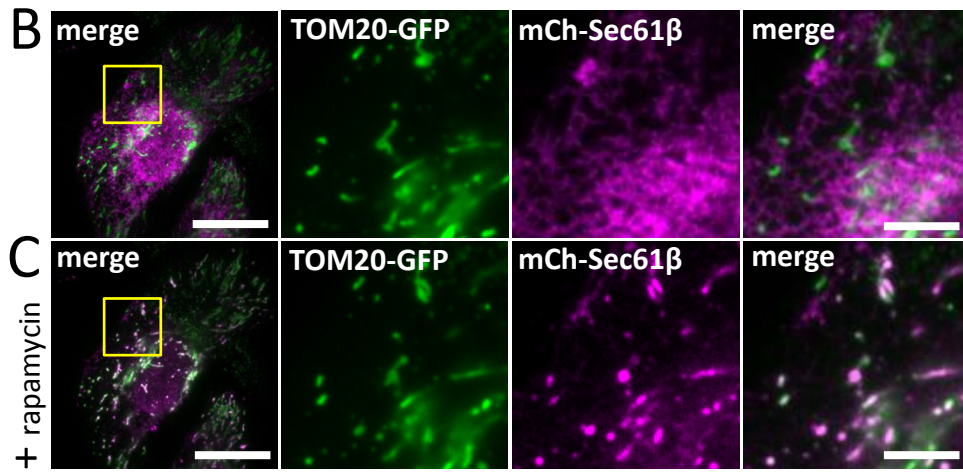
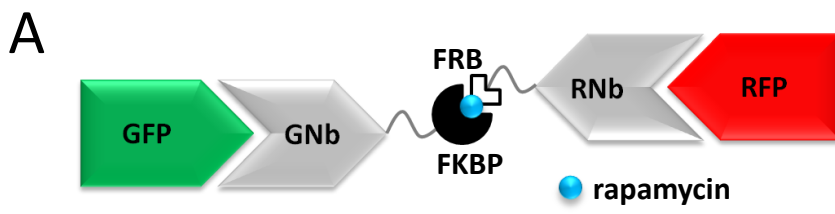


Figure 16.

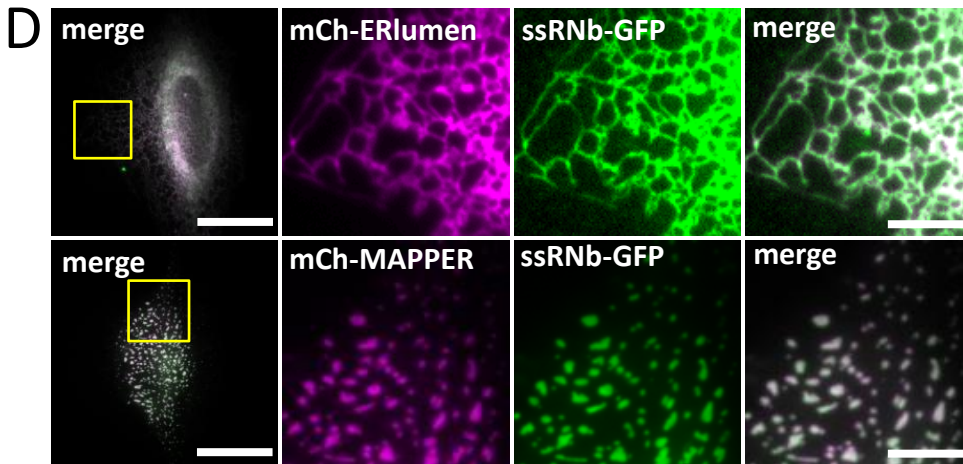
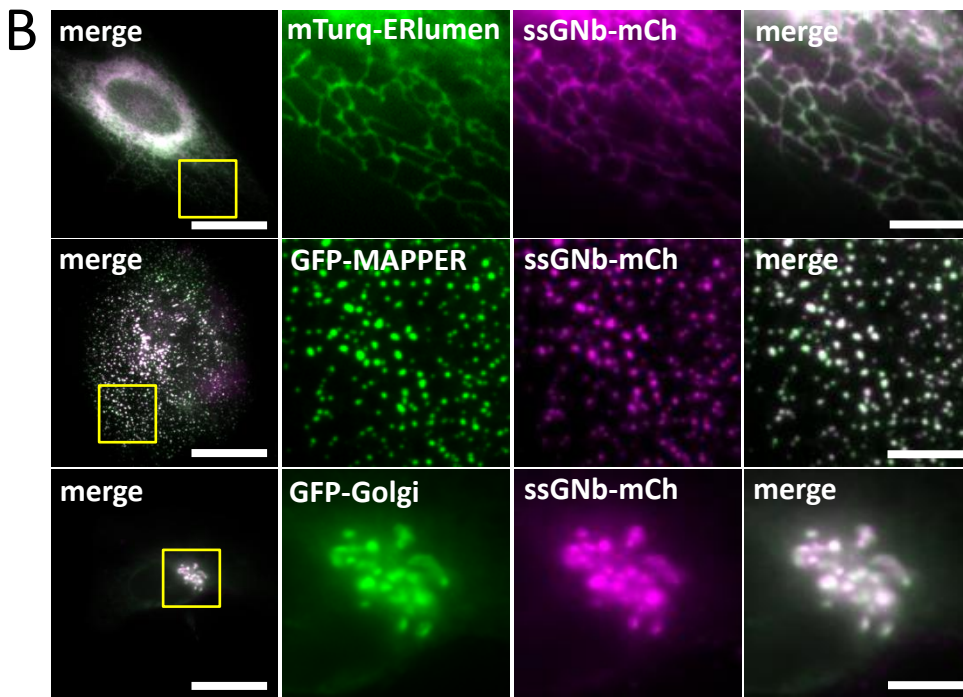


Figure 17.

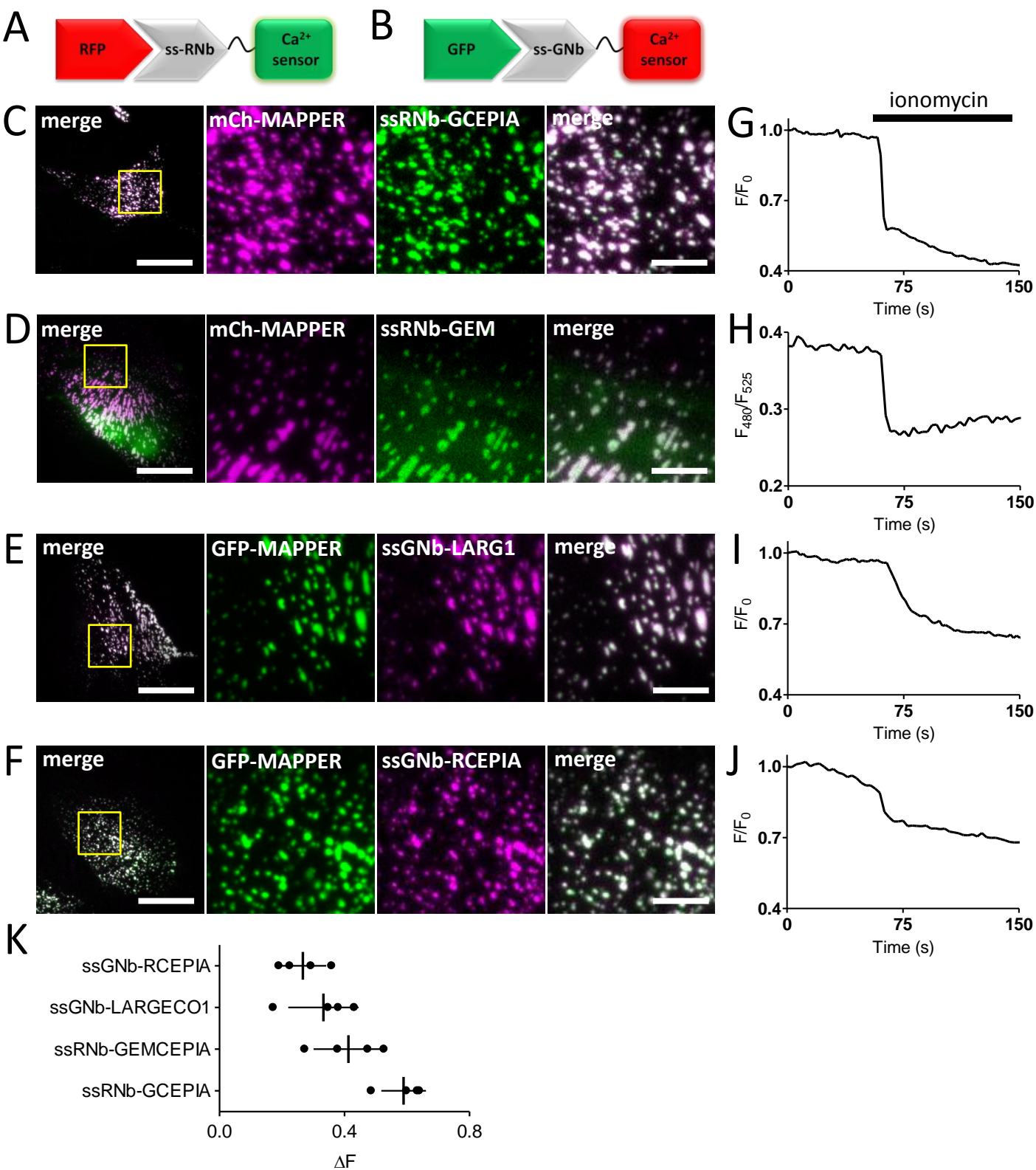


Figure 18.